

**A DENSITY FUNCTIONAL STUDY ON STRUCTURAL,
ELECTRONIC, CHEMICAL AND OPTICAL PROPERTIES OF
Ag-X, Al-X AND Cu-X [X=Li, Na, K] NANO-ALLOYS
FOR OPTO-ELECTRONIC AND CATALYTIC
APPLICATIONS**

SHAIKAT DEBNATH

**FACULTY OF ENGINEERING
UNIVERSITY OF MALAYA
KUALA LUMPUR**

2015

**A DENSITY FUNCTIONAL STUDY ON
STRUCTURAL, ELECTRONIC, CHEMICAL AND OPTICAL
PROPERTIES OF Ag-X, Al-X AND Cu-X [X=Li, Na, K]
NANO-ALLOYS FOR OPTO-ELECTRONIC AND
CATALYTIC APPLICATIONS**

SHAIKAT DEBNATH

**DISSERTATION SUBMITTED IN FULLFILLMENT OF THE
REQUIREMENTS FOR THE DEGREE OF MASTER OF ENGINEERING
SCIENCE**

FACULTY OF ENGINEERING

UNIVERSITY OF MALAYA

KUALA LUMPUR

2015

Family is not an important thing, it is everything.

- Michael J. Fox

Apart from my family, I would like to dedicate this thesis towards the famous geochemist Clair Cameron Patterson, the scientist, who fought all through his life to make our mother earth a better living place.

University of Malaya

ORIGINAL LITERARY WORK DECLARATION

Name of Candidate: **Shaikat Debnath**

Registration/Matric No: **KGA130007**

Name of Degree: **Master of Engineering Science**

Title of Dissertation (“this Work”): **A DENSITY FUNCTIONAL STUDY ON ELECTRONIC AND OPTICAL PROPERTIES OF Ag-X, Al-X AND Cu-X [X=Li, Na, K] NANOALLOYS FOR OPTO-ELECTRONIC AND CATALYTIC APPLICATIONS**

Field of Study: **Nanomaterials**

I do solemnly and sincerely declare that:

- (1) I am the sole author/writer of this Work;
- (2) This Work is original;
- (3) Any use of any work in which copyright exists was done by way of fair dealing and for permitted purposes and any excerpt or extract from, or reference to or reproduction of any copyright work has been disclosed expressly and sufficiently and the title of the Work and its authorship have been acknowledged in this Work;
- (4) I do not have any actual knowledge nor ought I reasonably to know that the making of this work constitutes an infringement of any copyright work;
- (5) I hereby assign all and every rights in the copyright to this Work to the University of Malaya (“UM”), who henceforth shall be owner of the copyright in this Work and that any reproduction or use in any form or by any means whatsoever is prohibited without the written consent of UM having been first had and obtained;
- (6) I am fully aware that if in the course of making this Work I have infringed any copyright whether intentionally or otherwise, I may be subject to legal action or any other action as may be determined by UM.

Candidate’s Signature

Date:

Subscribed and solemnly declared before,

Witness’s Signature

Date:

Name:

Designation:

ABSTRACT

Over the past few decades, the progress in nanotechnology has impacted every aspect of science and technology. Among all the physical and chemical properties of the nanomaterials, the optical characteristics are of special interest because of their plasmonic phenomenon. Among the conventional plasmonic materials, Ag and Au are the mostly used. However, their high interband transition losses in optical frequencies and high price are restricting them from extensive commercial usage. Apart from Ag and Au, Cu and Al can come as low cost alternatives, which exhibit interesting plasmonic behavior. But unfortunately, none of them display optical properties as good as silver and gold. In contrast, it is reported that Li, Na and K possess the best plasmonic quality among all metals reported to date. But due to their very high reactivity towards air and water, it is very challenging to use their nanoparticles solely. Thus, in this work we have proposed Ag-X, Al-X and Cu-X [X=Li, Na, K] nanoalloys, whereas Ag-X is a potential improvement over Ag and Al-X and Cu-X nanoalloys can be considered as the low cost alternative of silver and gold. To evaluate the structural and electronic stability, chemical and optical properties of the upper-mentioned nanoalloys, a 13-atoms core-shell structure is selected as the quantum model, while Accelrys Materials studio is used for the density functional (DFT) calculations. In the framework of DFT, the geometrical stability of all the nanoalloys is checked through vibrational analysis and bond length comparison, which is followed by binding energy and HOMO-LUMO gap calculations to ensure the electronic stability. Later ionization potential and electronic affinity of the nanoalloys were calculated to predict their chemical nature. Finally, time dependent density functional calculations are carried out to observe the optical absorption spectra of the clusters, which was followed by partial density of states calculations. From the calculations, it is evident that all of the Li and

Na doped clusters have exhibited higher chemical stability, whereas their anions are found very reactive. Thus, all of the aforesaid Li and Na doped clusters can be excellent potential for catalytic applications. In addition, doping has yielded significant changes in the optical absorption spectra of the nanoalloys. For the Ag-X and Cu-X nanoalloys, noticeable improvement was observed in absorption intensity in visible and UV-Vis optical ranges as a result of doping. Typically, solar cells absorb light in the visible and UV-Vis regions, hence these Ag-X and Cu-X clusters can bring attention-grabbing heightening as a replacement of silver and gold nanoparticles in the thin film solar cells, as well as other opto-electronic applications. On the contrary, Al-X clusters are found to exhibit remarkable wide optical absorption band gap in UV optical spectra, for why it will be an excellent potential for UV-absorption applications such as UV-therapy, UV-coating etc. Thus it can be concluded that all of the Ag-X, Al-X and Cu-X [X=Li, Na, K] nanoalloys have outstanding electronic and optical properties and can be excellent potential for the applications in opto-electronics and catalysis.

ABSTRAK

Melangkaui beberapa dekad yang lepas, kemajuan dalam nanoteknologi telah meninggalkan kesan terhadap setiap aspek sains dan teknologi. Antara setiap sifat fizikal dan kimia bahan nano, ciri optikal menarik minat istimewa kerana fenomena plasmoniknya. Antara bahan-bahan plasmonik konvensional, perak dan emas adalah bahan yang digunakan kebanyakannya sehingga kini. Namun, kehilangan transisi antara jalur tinggi dalam frekuensi optikal dan harga yang tinggi menghalang mereka dari penggunaan komersil secara ekstensif. Selain dari perak dan emas, tembaga dan aluminium juga boleh menjadi alternatif kos rendah, yang mana mempamerkan perilaku plasmonik yang menarik. Tetapi malangnya, tiada dari Cu atau Al menunjukkan sifat optikal sebaik perak dan emas. Secara kontras, Li, Na, dan K dilaporkan mempunyai kualiti plasmonik terbaik antara semua logam dilaporkan sehingga kini. Tetapi oleh kerana ia sangat reaktif dengan udara dan air, adalah sangat mencabar untuk menggunakan partikel nano itu secara tunggal. Oleh itu, dalam kerja ini, kami telah mencadangkan aloi nano Ag-X, Al-X dan Cu-X [X=Li, Na, K], yang mana Ag-X adalah potensi penambahbaik terhadap Ag, dan aloi nano Al-X dan Cu-X boleh dianggap alternatif kos rendah kepada perak dan emas. Untuk menilai kestabilan struktur dan elektronik, sifat kimia dan optikal aloi nano disebut di atas, teras-kekerang 13-atom dipilih sebagai model kuantum, sementara Accelrys Materials Studio digunakan untuk pengiraan teori fungsi ketumpatan (DFT). Dalam rangka kerja DFT, kestabilan geometri semua aloi nano diperiksa melalui analisis getaran dan perbandingan panjang ikatan, diikuti dengan tenaga ikatan dan pengiraan beza HOMO-LUMO untuk memastikan kestabilan elektronik. Kemudian keupayaan pengionan dan keafinan elektronik aloi nano dikira untuk meramal sifat kimia mereka. Akhirnya, pengiraan fungsi ketumpatan

bersandar masa dijalankan untuk melihat spektrum penyerapan optik kluster itu, diikuti dengan pengiraan ketumpatan keadaan separa. Daripada pengiraan itu, bukti menunjukkan semua kluster yang didopkan dengan Li dan Na telah mempamerkan kestabilan kimia yang tinggi, juga anionnya adalah sangat reaktif. Dengan itu, kluster doped dengan Li dan Na boleh menjadi potensi besar untuk aplikasi mungkin. Tambahan pula, dop telah menghasilkan perubahan signifikan dalam spektrum penyerapan optikal aloi-aloi nano itu, dibandingkan dengan aloi yang tidak didop. Untuk aloi nano Ag-X dan Cu-X, peningkatan yang ketara telah dilihat dalam keamatan penyerapan rantau optikal cahaya nampak dan UV-Vis hasil dari dop. Kebiasaannya, sel solar menyerap cahaya dalam rantau cahaya nampak dan UV-Vis, oleh kerana kluster Ag-X dan Cu-X mampu mengambil tumpuan sebagai pengganti partikel nano perak dan emas dalam sel solar nipis, dan juga aplikasi-aplikasi opto-elektronik yang lain. Secara kontra, Al-X dilihat mempamerkan ruang jalur penyerapan optikal yang lebar dalam spektrum UV, dengan ini ia berpotensi untuk aplikasi penyerapan UV seperti terapi-UV, salut-UV dan sebagainya. Jadi boleh disimpulkan bahawa semua aloi nano Ag-X, Al-X dan Cu-X [X=Li, Na, K] mempunyai sifat elektronik dan optikal yang menonjol dan berpotensi dalam aplikasi opto-elektronik dan pemangkinan yang hebat.

ACKNOWLEDGEMENT

First and foremost, I would like to thank Almighty to be the most gracious and merciful all through my life. I would also like to express my deepest love and affection towards my beloved family. Whatever I am today, it is only because of them.

Brad Henry said, “*A good teacher can inspire hope, ignite the imagination, and instill a love of learning.*” And I have got all these things from my respected supervisor Dr. Suhana Mohd Said. She was not only the supervisor for me, rather the ‘friend, guide and philosopher’ who has been the most influential teacher of my whole life. Her contributions, intellectual guidance, encouragement and massive compassionate support throughout my masters’ research have made it possible to achieve many precious successes during the candidature and the journey is still going continuing. I would also like to thank my co-supervisor, Dr. Azizah Mainal for her profound advice and continuous support during my research. Also, I want to thank Dr. Mohd Faizul Bin Mohd Sabri for his advices and support throughout my research. Special thanks to Dr. Abhijit Chatterjee from Accelrys Materials Studio for his continuous support.

During my research for the last two years, I was very lucky to get enormous help from many researchers from all part of the world. Heartiest thanks go to all. Special thanks towards Professor Rene Fournier from York University, Canada, Dr. David Levine, an independent researcher from USA, Dr. Franck Rabilloud from Université de Lyon, France and Dr. Martin Blaber from Northwestern University, USA for their prudent expertise and kind support.

I deeply appreciate the High Impact Research (HIR) for providing full financial support to carry out my research work. In addition, I cordially thank my core-organization, “Bangladesh Power Development Board, Ministry of Power, Energy and Mineral

Resources, Government of Peoples' Republic of Bangladesh" for approving my study-leave for my Masters' research.

Appreciations also go to the entire SSE and NME group members for making the laboratory an enjoyable place to work and live in. Special thanks go to Mamun vai and the Bad-Man Faris for their constant support. I would also like to thank Ovik, Robi, Asiq, Munaz, Megat, Azlan, Aiysha, Fini, Mohammad and Basir. Last, but not the least, I like to thank my childhood friend Surajit Das Barman. Without their help, certainly I can't carry out my research and life in Malaysia.

Last, but not the least, I like to thank my Malaysian Gooner friends with whom I watched Arsenal FC matches week in, week out for the last 2 years!

TABLE OF CONTENTS

LIST OF FIGURES	xii
LIST OF TABLES	xiv
LIST OF ABBREVIATIONS	xvi
CHAPTER 1 INTRODUCTION	01
1.1. Objectives	05
CHAPTER 2 LITERATURE REVIEW	06
2.1. Background	07
2.2. The ideal plasmonic material	08
2.3. Conventional plasmonic material	12
2.4. Selection criteria for alternative plasmonic materials	14
2.5. Alternative plasmonic materials	16
2.6. Bimetallic nanoalloys for potential plasmonic materials.....	21
2.7. 13-atoms Icosahedral structures as the quantum model of Ag-X, Cu-X and Al-X nanoalloys.....	24
2.8. Summary	26
CHAPTER 3 METHODOLOGY	28
3.1. 13-atoms core-shell structure of Ag-X, Al-X and Cu-X nanoalloys	29
3.2. Geometrical optimization and stability calculation	30
3.2.1. Geometry optimization	30
3.2.2. Harmonic vibrational frequency	30
3.2.3. Bond length comparison	32
3.3. Electronic and chemical stability calculation	32

3.4. Optical absorption calculation	35
3.5. Computational Method	36
CHAPTER 4 RESULTS AND ANALYSIS	39
4.1. Structural stability and the electronic, chemical and optical properties of 13-atoms icosahedral $Ag_{12}X$ structures	40
4.1.1. Geometrical structure and energetic stability	41
4.1.2. Electronic properties	46
4.1.3. Optical absorption spectra	50
4.2. Structural stability and the electronic, chemical and optical properties of 13-atoms decahedral $Ag_{12}X$ structures	54
4.2.1. Geometrical structure and energetic stability	54
4.2.2. Electronic properties	58
4.2.3. Optical absorption spectra	61
4.3. Structural stability and the electronic, chemical and optical properties of 13-atoms icosahedral $Al_{12}X$ and $Cu_{12}X$ structures	65
4.3.1. Geometrical structure and energetic stability	66
4.3.2. Electronic properties	67
4.3.3. Optical absorption spectra	71
4.4. Summary	76
CHAPTER 5 CONCLUSION	79
APPENDIX A PULICATIONS AND CONFERENCE	83
REFERENCES	84

LIST OF FIGURES

Figure 2.1. Quality factor, Q_{LSP}^{\max} comparison among all the metals of the periodic chart. All the frequencies are in eV.	17
Figure 2.2. Optimized geometrical structure of the metals	20
Figure 2.3. Optimized absorption spectra for nanoshells with radii and aspect ratios given in the Table-2.2 (A) without surface scattering, (B) with surface scattering	20
Figure 3.1. (a) Ag_{13} structure of icosahedral symmetry, (b) Na-doped into the core, (c) Na-doped into the shell	29
Figure 4.1. Optimized geometry of the icosahedral Ag_{13} and the $Ag_{12}X$ clusters	43
Figure 4.2 (a). Optical absorption spectra of icosahedral Ag_{13}	50
Figure 4.2 (b). Optical absorption spectra of c-doped $Ag_{12}X$ nanoalloys	51
Figure 4.2 (c). Optical absorption spectra of s-doped $Ag_{12}X$ nanoalloys	51
Figure 4.3 (a). PDOS of Ag_{13}	53
Figure 4.3 (b). PDOS of c-doped $Ag_{12}Li$	53
Figure 4.3 (c). PDOS of s-doped $Ag_{12}Li$	53
Figure 4.4. Optimized geometry of the decahedral Ag_{13} and the $Ag_{12}X$ clusters	56
Figure 4.5 (a). Optical absorption spectra of decahedral Ag_{13}	62
Figure 4.5 (b). Optical absorption spectra of c-doped $Ag_{12}X$ nanoalloys	63

Figure 4.5 (c). Optical absorption spectra of v-doped Ag_{12}X nanoalloys	63
Figure 4.5 (d). Optical absorption spectra of s-doped Ag_{12}X nanoalloys	63
Figure 4.6. PDOS of (a) decahedral Ag_{13} , (b) c-doped Ag_{12}Li , (c) v-doped Ag_{12}Li , (d) s-doped Ag_{12}Li	64
Figure 4.7. Optimized geometry of the decahedral Al_{12}X and the Cu_{12}X clusters	77
Figure 4.8. Absorption spectra of Cu_{13} and Cu_{12}X clusters	72
Figure 4.9. Absorption spectra of Al_{13} and Al_{12}X clusters up to 6 eV	73
Figure 4.10. Absorption spectra of Al_{13} and Al_{12}X clusters up to 11 eV	74

LIST OF TABLES

Table 2.1. Optical constants of metals	18
Table 2.2. Shell geometries for optimized absorption with and without surface scattering	19
Table 4.1. Vibrational frequency of the Ag_{13} and Ag_{12}X clusters	44
Table 4.2. Comparison of average bond lengths of the nanoalloys	44
Table 4.3. Thermodynamic properties of the c-doped Ag_{12}X clusters	45
Table 4.4. Thermodynamic properties of the s-doped Ag_{12}X clusters	45
Table 4.5. Binding energy (BE), vertical ionization potential (VIP), vertical electron affinity (VEA) and HOMO-LUMO gaps of the undoped icosahedral Ag_{13} and c-doped Ag_{12}X clusters	48
Table 4.6. Binding energy (BE), vertical ionization potential (VIP), vertical electron affinity (VEA) and HOMO-LUMO gaps of the undoped icosahedral Ag_{13} and s-doped Ag_{12}X clusters	48
Table 4.7. Bond length comparison among the undoped and the doped clusters	57
Table 4.8. Binding energy (BE), vertical ionization potential (VIP), vertical electron affinity (VEA) and HOMO-LUMO gaps for decahedral Ag_{13} and c-doped Ag_{12}X clusters	59
Table 4.9. Binding energy (BE), vertical ionization potential (VIP), vertical electron affinity (VEA) and HOMO-LUMO gaps for v-doped and s-doped Ag_{12}X clusters	59

Table 4.10. Lowest and highest vibrational frequency of the $Al_{12}X$ and $Cu_{12}X$ clusters	67
Table 4.11. Binding energy (BE), vertical ionization potential (VIP), vertical electron affinity (VEA) and HOMO-LUMO gaps of the undoped Cu_{13} and $Cu_{12}X$ clusters	68
Table 4.12. Binding energy (BE), vertical ionization potential (VIP), vertical electron affinity (VEA) and HOMO-LUMO gaps of the undoped Al_{13} and $Al_{12}X$ clusters	69

LIST OF ABBREVIATIONS

NP	=	Nanoparticle
DFT	=	Density Functional Theory
FDDT	=	Finite Difference Time Domain
TDDFT	=	Time Dependent Density Functional Theory
DDA	=	Discrete Dipole Approximation
SPR	=	Surface Plasmon Resonance
LSP	=	Localized Surface Plasmon
SCF	=	Self-Consistent Field
GGA	=	Generalized Gradient Approximation
PBE	=	Perdew-Burke-Ernzerhof
DNP	=	Double Numeric Quality basis set
Ih	=	Icosahedral
Dh	=	Decahedral
Oh	=	Octahedral
c-doped	=	Core-doped
s-doped	=	Surface-doped
v-doped	=	Vertex-doped
BE	=	Binding Energy
IP	=	Ionization Potential
VIP	=	Vertical Ionization Potential
EA	=	Electron Affinity
VEA	=	Vertical Electron Affinity
MO	=	Molecular Orbital

HOMO	=	Highest Occupied Molecular Orbital
LUMO	=	Lowest Unoccupied Molecular Orbital
PDOS	=	Partial Density of States
UV	=	Ultraviolet
UV-Vis	=	Ultraviolet-Visible
STM	=	Scanning Tunneling Microscope

CHAPTER 1

INTRODUCTION

We are at the very beginning of time for the human race. It is not unreasonable that we grapple with problems. But there are tens of thousands of years in the future. Our responsibility is to do what we can, learn what we can, improve the solutions, and pass them on.

The above-mentioned famous quote is from the Nobel-prize winning physicist Richard Phillips Feynman. Despite being criticized in developing atomic bomb for Second World War, he was more popular being the Father of Nanotechnology. The ideas and concepts behind nanoscience and nanotechnology started with his talk entitled “*There’s Plenty of Room at the Bottom*” at an American Physical Society meeting at the California Institute of Technology on December 29, 1959, long before the term nanotechnology was used. In his talk, Feynman described a process in which scientists would be able to manipulate and control individual atoms and molecules. Over a decade later, in his explorations of ultra-precision machining, Professor Norio Taniguchi coined the term nanotechnology. It was not until 1981, with the development of the scanning tunneling microscope that could "see" individual atoms. And there begins a new era for modern technology, which is popularly known as Nanotechnology.

After 55 years of that famous speech from Richard Feynman, here I am writing my Masters’ thesis on the potential of several bimetallic nanomaterials as alternatives of expensive silver and gold, to play my part in the accomplishment of what Richard

Feynman said in his above mentioned quote: “*Our responsibility is to do what we can, learn what we can, improve the solutions, and pass them on.*”

After the first concept of nanomaterials comes from Richard Feynman in 1959, it was Professor Norio Taniguchi who was the first person to introduce the term “Nanotechnology” in 1974. Since then, nanotechnology, as well as nanomaterials has been in the core of research interest for the science community for its fascinating physical and chemical properties. Apparently, it was in the years of 2000, the world has observed that applications of nanomaterials in the commercial products, although at that time it was only limited to very few commercial products such as food packaging, sunscreen, cosmetics and textiles. But it took only 10-15 years, when in today’s world nanomaterials have set versatile platform for a range of diverse applications ranging from photovoltaic (Photiphitak, Rakkwamsuk, Muthitamongkol, Sae-Kung, & Thanachayanont, 2011) to biological (Singh et al., 2014) and chemical sensors (Yu, Kudrinskiy, Olenin, & Lisichkin, 2008) and catalysis (Rashid & Mandal, 2007).

Among the nanomaterials used so far, silver and gold have been the most popular metals because of their distinct physical, electronic and chemical properties. But using silver and gold nanoparticles is not commercially competitive due their high price and scarcity in the earth’s crust. In this situation, while looking at the alternative nanomaterials, being cheap and abundant, both of Al and Cu looks impressive. But the problem is neither the Al or Cu exhibit plasmonic quality which is as good as silver and gold. In this situation, bimetallic nanomaterials can bring some attractive alternatives.

Bimetallic nanoclusters, which are the aggregation of two types of metal atoms of nanoparticle size, have been utilized as key components in many catalytic, optical and magnetic devices. It has been subject to an interest of both theoretical and experimental research for its distinct physical and chemical properties (Zhurkin, Van Hoof, & Hou, 2007) Now a days, there is growing interest in bimetallic nanoparticles, compared to monometallic nanoparticles because bimetalization can offer space of improvement in

optical, catalytic and magnetic performance over the original pure mono-metal nanoparticles and can create new properties. In addition, molecular tuning of these bimetallic nanoclusters may give rise to novel properties which are not realized in bulk or, monometallic nanoparticles. (Ferrando, Jellinek, & Johnston, 2008; Rodriguez & Goodman, 1992) The properties of these bimetallic nanoclusters are not solely size-dependent, rather the chemical composition and molecular arrangement significantly affect their specific structural, (Chen et al., 2007; Derosa et al. 2001; Yuan et al. 2008; Yuan et al 2005) electronic, (Derosa et al., 2001; Yuan et al., 2005) optical (Chen et al., 2007; Schwartzberg & Zhang, 2008) and magnetic properties (Janssens et al.,2005) which has led to a technological interest in catalysis (Barnard et al., 2011; Kaizuka et al., 2010) and also in the application and development of new nano-devices for electronics. (Ferrando et al., 2008)

Amongst the characteristics of bimetallic nanoclusters, optical properties are of special interest because of its plasmonic properties. The nanoparticles which support Surface Plasmon Resonance (SPR) are called plasmonic metal nanoparticles, whereas SPR is defined as the collective oscillation of electrons in a solid or liquid stimulated by incident light. The resonance condition for SPR is established when the frequency of light photons matches the natural frequency of surface electrons oscillating against the restoring force of positive nuclei. (Zeng et al., 2011) SPR is accountable for a series of phenomena which are completely unique for every nanometal when the nanometal is a subject of interaction with light.

At the times, when alternative nanomaterials with plasmonic properties are looked for, alkali metals are the elemental free-electron metals, which have been identified as excellent potential for plasmonic nanometal. It is reported (Blaber, Arnold, & Ford, 2009b, 2010) that sodium and potassium have the highest absorption efficiency (Q_{abs}),

along with very low inter-band transition losses at optical frequencies amongst all the nonmetals that have been tested yet. In fact, these transition losses are comparable or even better than that of silver or, gold along with their property of exhibiting the strongest free-electron-like-behavior, which result in very prominent SPR in visible-UV range. (West et al., 2010) But unfortunately, as alkali metals like sodium and potassium are very much reactive and easily oxidizes upon their bringing in air, the realistic chances of using them as mono-metal nanomaterial in commercial products are really narrow even though, they have excellent plasmonic properties. In such situation, bimetalization of alkali metals with silver, copper and aluminum can be an excellent way to use the remarkable plasmonic properties of alkali metals as bimetalization can allow us to control the reactivity of the alkali metals with air and water to an acceptable limit.

Therefore, in this work, we have doped X nanomaterials (X=Li, Na and K) into silver, aluminum and copper to form Ag-X, Al-X and Cu-X nano-alloys. Later, comprehensive study is done with a theoretical approach where density functional theory (DFT) is used as the functional method. The geometrical and electronic stability of the mentioned nano-alloys are checked to ensure the long term stability for the targeted applications. Moreover, chemical and optical properties of the mentioned nano-alloys have been explored to check their potential for the applications in the field of opto-electronics and catalysis. Thus, the objectives of this research work can be summarized in the following way:

1.1. Objectives

1. The primary objective of this research work is to find plasmonic materials as alternatives of silver and gold. For that Ag-X, Al-X and Cu-X [X=Li, Na, K] have been suggested.

2. The electronic and chemical properties of the mentioned alloys will be checked for its probable application in catalysis.
3. The optical properties of the mentioned alloys will be explored for its potential opto-electronic applications such as plasmonic solar cells.

After this brief introduction, the later part of this thesis is followed by the following subdivisions:

Chapter 2 describes the literature review where the short comings of the currently used nanomaterials and the probable alternative nanomaterials as well as potential bimetallic nano-alloys are extensively discussed with previously reported theoretical and experimental reasoning. Detailed explanation regarding the theoretical quantum model is presented as well, to justify the theoretical approach proposed.

Chapter 3 presents the design procedure of the proposed theoretical method and simulation technique used to execute the chemical and optical performances of the nanoalloys.

Chapter 4 explains the simulated and measured results obtained from the proposed DFT calculation, where the electronic, chemical and optical properties of the nano-alloys are presented with detail clarification to test their potential in opto-electronic and catalytic applications.

Chapter 5 outlines the remarks of conclusion of this work precisely and also describes the scope of future work by using this set of nano-alloys.

CHAPTER 2

LITERATURE REVIEW

And that because the moving parts are a million times smaller than the ones we are familiar with, they move a million time faster, just as a smaller tuning fork produces a higher pitch than a large one.

The above-mentioned quote is from the famous American engineer Kim Eric Drexler, a pioneer in the history of nanotechnology. It was in the years of 1980, when he became the first one to bring the technological significance of nano-scale phenomena and let the world know about the potential of ultra-fast nano-devices through specific control in molecular scale. Since the first concept of nanotechnology came in 1959 by Richard Feynman, it was only restricted as a physics-concept but it was the technological interest in nanomaterials that has brought it into intense interest. In today's world, we now can easily see that the extensive applications of the nano-materials are playing the pivotal role behind the concentrated interest in nanomaterials from both of the theoreticians and the engineers. In this research, opto-electronic devices (such as thin film solar cells) and catalytic applications are the major motivations when some new nano-alloys for the above mentioned application fields have been proposed. In this chapter, the literature review will be discussed which will start with the theoretical concept of ideal plasmonic nanomaterials and the drawbacks of the currently used nanomaterials. Later it will be followed by the probable alternative bimetallic nano-alloys with comprehensive discussion of previously reported theoretical and experimental reasoning. Also, detailed explanation regarding the proposed theoretical quantum model is presented for justification of the theoretical approach used.

2.1. Background

Over the past few decades, the progress in nanotechnology has impacted every aspect of science and technology. Among all the physical and chemical properties of the nanomaterials, the optical characteristics are of special interest because of their plasmonic phenomenon. Thus, plasmonic metamaterials can be described as the metallic nanoparticles that exploit surface plasmons, which are produced from the interaction of light with metal-dielectric materials. This plasmon phenomenon is characteristically originated from the collective oscillations of the free charges in a material due to an applied electromagnetic field. For this, plasmonic devices typically need metallic components as the metals have an abundance of free electrons. These free electrons deliver the negative real permittivity which is the most essential part for any plasmonic material. (Merten et al., 2007) At the same time metals have some unavoidable problems such as almost all the metals exhibit large losses, especially in the visible and ultra-violet band. The main reason behind this high loss is due their interband electronic transitions. Interestingly, metals with highest conductivities also suffer from these interband losses at their optical frequencies. (Johnson & Christy, 1972; Marton & Jordan, 1977) Moreover, all metals are more or less very reactive to air and water and this reactivity even increases when they are as small as nanoparticles. Thus, the fabrication of metal nanoparticles and ensuring them are non-reactive to air and water is quite challenging. On the other hand, organic materials typically do not exhibit any plasmonic behavior at all, given the fact that generally organic materials do not have abundant free electrons in their outer shell. Therefore, despite of having some shortcomings, at the moment metals are the only option available for us. So, first the theory of ideal plasmonic nanomaterials will be examined, which will be followed by

the list of the popular metallic nanoparticles which exhibit plasmonic properties and currently in use of different plasmonic applications.

2.2. The ideal plasmonic material

Plasmonic metamaterials are incarnations of materials first proposed by Victor Veselago, a Russian theoretical physicist, in 1967. Also known as left-handed or negative index materials, the proposed materials were theorized to exhibit optical properties opposite to those of glass, air. These have been termed positive index-materials of our everyday world. In particular, energy is transported in a direction opposite to that of propagating wave-fronts, rather than traveling in lockstep, as is the case in positive index materials. As a result, when juxtaposed with a positive index material, negative index materials were predicted to exhibit counterintuitive properties, like bending, or refracting, light in unnatural ways. (Lezec et al., 2007)

Understanding of the plasmonic behavior of metallic nanoparticles it is necessary to correlate the metal's interaction with electromagnetic waves, i.e. the polarization of a metal. A metal's polarization with respect to the incoming electromagnetic wave can either be electrical or magnetic. Typically, the magnetic polarization have very negligible influence in the plasmonic behavior of the materials, hence the electrical polarization is our prime interest (West et al., 2010). This electrical polarization of any material which is completely liable for the plasmonic response of any material is described by the complex dielectric function, $\varepsilon(\omega) = \varepsilon'(\omega) + i\varepsilon''(\omega)$.

Generally, it is the sign of the real part of the permittivity that distinguishes a dielectric material from a plasmonic material. The dielectric materials display a positive value of permittivity, whereas the plasmonic materials exhibit negative permittivity in the

frequency range of interest. In another way, it is the real part of the dielectric function, $\epsilon'(\omega)$ determines the wavelength of light at which the plasmonic resonance will occur. On the other hand, the complex part $\epsilon''(\omega)$ is liable for the optical losses of a material. Thus the higher the value of the imaginary permittivity, the higher will be the optical losses; hence small values of $\epsilon''(\omega)$ is the primary need for a low loss plasmonic material. (Keast et al., 2014) Thus, an ideal plasmonic material would possess a negative real part of the permittivity and a zero imaginary part of the permittivity (or zero optical losses) in the spectral range of interest. In addition to the requirements on the optical properties of a good plasmonic material, a useful plasmonic material should be chemically stable, mechanically robust, and easy to fabricate and integrate with existing semiconductor devices (G. V. Naik et al., 2013).

Before the summarization of the necessary properties of the ideal plasmonic nanomaterials, it is needed to understand the origin of the optical properties of the plasmonic nanomaterials. Loss mechanisms in the near-infrared (NIR), visible, and soft-UV frequency ranges may be broadly classified as arising from phenomena related to conduction electrons (intraband effects), core electrons (interband effects) and lattice vibrations (phonons). Because phonon losses in solids are several orders of magnitude smaller than those due to electrons at NIR and visible frequencies, we restrict our discussion to only interband and intraband contributions. (Drachev et al., 2008; Trivedi & Ashcroft, 1988) Losses due to intraband contributions primarily arise from conduction-band electrons. Since the conduction electrons have a near continuum of available states, their interaction with an electromagnetic field is well described by classical theory. Drude theory describes this phenomenon by treating conduction electrons as a three-dimensional free-electron gas (Drude, 1900). The generalized Drude

theory describing the permittivity of a material due to its conduction electrons is stated in Equation 2.1(a):

$$\varepsilon(\omega) = \varepsilon' + i\varepsilon'' = \varepsilon_b - \frac{\omega_p^2}{(\omega^2 + \gamma^2)} + i \frac{\omega_p^2 \gamma}{(\omega^2 + \gamma^2)\omega}, \quad 2.1(a)$$

$$\omega_p^2 = \frac{ne^2}{\varepsilon_0 m^*}. \quad 2.1(b)$$

In Equation 2.1(a), ε_b is the polarization response from the core electrons (background permittivity), ω_p is the plasma frequency, and γ is the Drude relaxation rate. The plasma frequency (ω_p) is given by Equation 2.1(b), where n is the conduction electron density, and the effective optical mass of the conduction electrons is m^* . In general, ε_b depends on wavelength (which is typically accounted by including the Lorentz oscillator terms) but for some spectral ranges it can be roughly approximated as constant. Also, γ can depend on the size of the plasmonic particle. For a small particle of size R , the plasmon relaxation rate can be affected by electron scattering at the boundary, leading to Equation 2.2:

$$\gamma = \gamma_\infty + A \frac{v_F}{R} \quad (2.2)$$

Here, γ_∞ is the bulk value, v_F is the Fermi velocity, R is the radius of a spherical particle and A depends on details of the scattering process with the order of unity (Persson, 1991). For simplicity, we assume that $\gamma = \gamma_\infty$.

Because plasmonic applications require materials with negative ε'' , Equation (2.1(a)) clearly indicates that this requirement is satisfied for materials with a plasma frequency higher than the desired frequency of application. Because metals tend to have large plasma frequencies and high electrical conductivities, they have traditionally been the materials of choice for plasmonic applications.

The unavoidable problem which every metal will experience is loss due to interband transitions. It occurs in optical frequencies, when electrons jump to higher energy levels due to absorption of incident photons. In metals, when a bound electron absorbs an incident photon, the electron can shift from a lower energy level to the Fermi surface or from near the Fermi surface to the next higher energy level. Both of these processes result in high loss at optical frequencies. Thus, an ideal plasmonic material should possess a negative real permittivity and absolutely zero optical loss, i.e. zero imaginary permittivity. However, in real world it is not possible to find out any material which will have an absolute zero value of its imaginary permittivity. Hence, a material with negative real permittivity and very small optical losses in desired frequency will make it a fantastic candidate as plasmonic material.

At this point, in order to incorporate the above mentioned mathematical summary with physical properties of a material, typically four electronic features are looked for in a material to check their plasmonic quality. These four features are as follows, which are quoted from the works of Blaber et al. (Blaber et al., 2009; Blaber et al., 2010).

- 1) The gradient of bands at the Fermi surface must be high enough to allow for an appropriate plasma frequency.
- 2) The Drude phenomenological damping term has to be lower than the plasma frequency.
- 3) The ‘core polarizability’ must be low.
- 4) The ratio between the optical gap and the plasma frequency must be proportional to the sharpness of the band edge itself. That is a material with a sharp band edge that reduces rapidly with increased frequency will perform better than a material where the band edge does not comprise the dominant transition mechanism.

Thus, we can conclude this part by stating that along with the above-mentioned electronic properties, an ideal plasmonic material should be electronically stable and chemically non-reactive, mechanically robust and should have an easy method for fabrication.

2.3. Conventional plasmonic materials

Among all the metals that have been used till date, silver and gold are the most commonly used materials due to their comparatively low optical losses in the visible and near-infrared (NIR) region. In fact, sheer portions of the theoretical and experimental works that have been done since the beginning of plasmonic material's research are either on silver or, gold. For example, the usages of silver have been demonstrated as negative refractive index material, hyperlens, (Liu et al.,2007) superlens (Fang et al., 2005) and optical transmission (Ebbesen et al.,1998). Apart from silver, gold is the other conventional plasmonic material which has been used as a negative refractive index nanomaterial in the NIR region and several Localized Surface Plasmon Resonance (LSPR) sensors (Dintinger et al., 2013; Shalaev et al., 2005; West et al., 2010).

Other than silver and gold, the uses of several other metals have also been observed but their usage was quite limited due to their high optical losses compared to silver and gold. For example, platinum and palladium are used in micro-devices as the catalytic plasmonic material (Baldelli et al., 2000; Tobiška et al., 2001). In addition, nickel films have been reported to have surface plasmon-coupled chemi-luminescence, which may merit the use of nickel in particular plasmonic applications. Moreover, copper and aluminum have been tested for several plasmonic based applications. Copper, being a cheaper option has the potential to replace silver and gold as it exhibits plasmonic

properties in the UV-Vis region, however both of its interband and intraband transition losses are significantly higher compared to that of silver and gold. Aluminum is another option but it absorbs light only in the UV region, hence its applications are strictly limited to UV region.

As previously mentioned, amongst the conventional plasmonic materials, silver and gold are the mostly used materials till date. In terms of optical losses, silver possesses the lowest loss in visible and NIR region. However, when the nano-fabrication is concerned, silver degrades comparatively quickly and the thickness threshold for uniform continuous films is around 12-13 nm which is a major barrier for transformation optic (TO) and several other micro and nano-devices. (Oates & Mücklich, 2005; Wei & Eilers, 2009) In addition, the dependence of silver's optical losses with the roughness of the surface has made it difficult in terms of usage in commercial devices. After silver, gold is the next most used plasmonic material which exhibit low optical losses in visible and NIR region. In a comparison with silver, gold is chemically more stable and is able to make a continuous nano-film of 1.5-7 nm thickness (Smith et al., 1999; West et al., 2010; Yagil et al., 1992). However, the losses of gold can be quite high, especially in the green to blue region of the visible spectrum.

Along with all these problems mentioned above, the main demerits of silver and gold are their extensive high prices and scarcity on earth, which eventually make them unsuitable for commercial applications. For this reason scientists and engineers have been looking for cheaper alternative plasmonic materials with low optical losses, which will be chemically stable and easy to fabricate in nano-scale as well.

2.4. Selection criteria for alternative plasmonic materials

From the previous part, it is now evident that metals are mostly used as conventional plasmonic materials due to their low ohmic losses i.e. their high DC conductivity. But when the interaction with optical frequencies is concerned, both of the interband and intraband transition losses of those materials play the pivotal role in selection criteria (Johnson & Christy, 1972). It is already stated that the ideal plasmonic materials require small value of their imaginary part of the permittivity. However, even if the interband losses get smaller, there are still intraband transition and scattering losses, which ultimately are increasing the overall losses. In order to realize the source of this problem, let us have a deeper look at the free-electron behavior of the metals. The relaxation time, γ (mentioned in Equation 2.2) is typically liable for the ohmic and scattering losses of a metal, which is also directly interrelated with the imaginary part of the Drude-permittivity (ϵ'') stated in Equation 2.1. A small ϵ'' can be achieved either by a small γ or by a smaller carrier concentration, or preferably both. (G. V. Naik et al., 2013) Attempts have been made to reduce γ in conventional plasmonic materials (noble metals) by cooling them to cryogenic temperatures (Bouillard et al., 2012). However, the improvement in losses is not sufficient for practical devices. In conventional plasmonic materials the carrier concentration is very large and this therefore significantly increases the value of ϵ'' in the NIR and visible regions. Decreasing the carrier concentration in these metals would be useful in significantly reducing the value of ϵ'' .

It is observed that the magnitude of ϵ' is usually high in noble metals (such as silver, gold) which is a major hindrance in designing micro-devices. These devices often require meta-molecules with a nearly balanced polarization response. (Bouillard et al., 2012; West et al., 2010) In other words, the polarization response from the metallic

components should be of the same order as that from the dielectric components within each meta-molecule. When the real parts of the permittivity and dielectric are of the same order, the geometric fill fractions of the metal and dielectric can be readily tuned to match the design requirements. On the other hand, if the magnitude of the real part of the permittivity of the metal is a few orders larger than that of the dielectric, the metal fill fraction in the meta-molecule will be a few orders smaller than that of the dielectric. This constraint would necessitate very tiny metal inclusions in the meta-molecule, which poses a number of problems especially in terms of successful nanofabrication. Thus, having smaller magnitudes of ϵ' for plasmonic materials would be advantageous in many applications (G. Naik et al., 2014). The origin of the large magnitude of ϵ' in noble metals can be traced to their very large carrier concentrations. From the Equation 2.1 and 2.2 it is clear that ϵ' is almost directly related with $\omega^2 p$ or carrier concentration (n). Thus, reduction in carrier concentration, as well as in plasma frequency will be an effective way to reducing the magnitude of ϵ' .

After discussing the influencing factors over the real and complex permittivity of plasmonic materials, the next focus is the most common parameter used to judge the optical response of any material which is the optical absorption efficiency (Q_{abs}). For a specific frequency, the higher will be the absorption efficiency, the better the material for any opto-electronic applications.

Apart from these testing-criteria mentioned, quality factor is another effective method to evaluate the proficiency of metals' performance in frequency dependent plasmonic applications. Despite that the quality factor is dependent on the size and shape of the metals, in the limit of low loss and the applicability of electronics, two generic limiting cases can be derived, (a) for localized surface plasmon (LSP) applications, which include the absorption efficiency of nano-sphere and nano-shells, and the resolving

power of a multilayer superlens and (b) for extent modes such as surface plasmon polaritons (SPP) and the LSP modes of ellipsoids. In our case, as we have been focusing on opto-electronic applications such as solar cells, we will be considering only LSP regarded quality factor, Q_{LSP} only. Now, the Q_{LSP} is defined as the ratio between the real and complex permittivity ($-\epsilon'/\epsilon''$), whereas the $Q_{\text{LSP}}^{\text{max}}$ is defined as follows:

$$Q_{\text{LSP}}^{\text{max}} = \frac{2(\omega_p^2 - 2\gamma^2[1 + 2\pi^{1/2}\alpha\sigma/\mu])^{3/2}}{3\gamma\omega_p^2\sqrt{3(1 + 2\pi^{1/2}\alpha\sigma/\mu)}} \quad (2.3)$$

Here, it worth mentioning that as like as absorption efficiency, for a material to be good in plasmonic performance, high values for the $Q_{\text{LSP}}^{\text{max}}$ is required. Hence, the high the value of the metal, the better it is for the plasmonic applications for that specific plasma frequency.

In light of the above discussions, it is apparent that low value for plasma frequency (ω_p) and relaxation time (γ) and large optical absorption efficiency (Q_{abs}) and quality factor ($Q_{\text{LSP}}^{\text{max}}$) are the primary prerequisites for a good plasmonic material. In the next section, we will compare several metals based on these mentioned properties to judge the overall scenario regarding the alternative plasmonic materials.

2.5. Alternative plasmonic materials

Despite that, loss-free ideal plasmonic metal can never be found on earth, other alternative of silver and gold to recompense the optical losses is elaborated here. As it is stated in the previous section, the alternative material search will be on the basis of absorption efficiency, plasma frequency and relaxation time.

The periodic chart in Figure 2.1 shows the maximum of Q_{LSP}^{\max} for all metals in their respective frequency of maximum Q_{LSP} . It is obvious that apart from silver and gold, group-IA alkali metals (Li, Na, K, Rb, and Cs) exhibit the highest quality factor whereas potassium (K) topped among the alkali metals. Other than alkali metals, Cu and Al have higher quality factors as well. Hence, in order to check the plasmonic aptitude, the following part will cover the comparative study among Ag, Au, Na, K, Al and Cu. (In spite of having good Q_{LSP} values, Rb, Cs and Fr are excluded from the list due to their extreme reactive nature towards water and oxygen.) To further study, Table-2.1 is presented with ω_p , γ and $\epsilon''_{ib}(0)$. For silver, the optical data of Johnson and Christy is used. For gold, the data of Weaver and Frederikse (Weaver & Frederikse, 2001) is used. The low frequency residual permittivity caused by interband transitions is calculated by fitting a skewed distribution function to the band edge in ϵ''_{ib} and a number of Gaussians to higher energy transitions. A numerical Kramers – Kronig integration is then performed to determine $\epsilon'_{ib}(0)$.

Li		Be		Element		B		C		Max Qlsp Key					
0.14*	0.20			Frequency of						0.00-2.99					
28.82	3.58			Max QLSP						3.00-3.99					
				* Frequency is at the limit of the available data						4.00-5.99					
				# Low frequency data not included						6.00-9.99					
										10+					
Na	Mg														
1.44	4.00														
35.09	9.94														
K	Ca	Sc	Ti	V	Cr	Mn	Fe	Co	Ni	Cu	Zn	Ga	Ge	As	Se
1.05	0.65*	0.3*	0.20	0.36	0.30	0.07*	0.10*	0.10*	0.15	1.75	3.60#	8.30			
40.68	3.63	1.02	2.58	4.27	2.16	1.16	2.48	2.69	2.71	10.09	3.59	3.41			
Rb	Sr	Y	Zr	Nb	Mo	Tc	Ru	Rh	Pd	Ag	Cd	In	Sn	Sb	Te
0.81	0.36*	1.48*	3.00	0.55	0.38		0.10*	0.30	0.10*	1.14	0.65#	5.10	2.25	3.50	
21.90	2.85	1.41	1.16	3.39	5.38		2.03	2.10	6.52	97.43	3.63	4.60	3.50	1.33	
Cs	Ba	Lan	Hf	Ta	W	Re	Os	Ir	Pt	Au	Hg	Tl	Pb	Bi	Po
0.51*	1.91		0.52*	0.58	0.30	0.10*	0.10*	0.40	0.35	1.40	4.20	3.20	5.95	3.50	
11.20	0.91		0.79	5.25	4.96	4.99	6.12	2.55	1.96	33.99	2.20	2.71	3.07	1.15	

Figure 2.1: Quality factor, Q_{LSP}^{\max} comparison among all the metals. All the frequencies are in eV (Blaber et al., 2010).

Table 2.1: Optical constants of metals. (Blaber et al., 2010; West et al., 2010)

Element	ω_p (eV)	γ (eV)	$\epsilon'_{ib}(0)$
Ag	9.62	0.0181	3.5
Au	8.55	0.0184	9.6
Al	12.5	0.0621	10.4
Cu	8.7	0.0700	6.7
Na	5.71	0.0276	1.09
K	3.72	0.0184	1.12

Table-2.1 reveals that Na and K exhibit the lowest values of plasma frequency and real interband permittivity. Thus, these alkali metals are expected to show low real permittivity; hence low optical losses will be associated as it is discussed earlier. With respect to relaxation time and from there it is obvious that both of the alkali metals are competitive with silver and gold with small relaxation time, i.e. low interband transition losses. Apart from the alkali metals, both of the Al and Cu have shown attraction-grabbing plasmonic behavior as well.

In light of the above discussions, it is obvious that alkali metals exhibit the best plasmonic performance amongst all metals. To further investigate the plasmonic behavior of the metals, the optical absorption is compared among the listed metals via the optical absorption efficiency against wavelength as shown in Figure 2.3. In addition, Table 2.2 represents numerical data of the shell geometries for optimized absorption with and without surface scattering, while Figure 2.2 shows the geometrical structure of the metals. The authors have used the numerical solution of Mie theory for calculating

the optical absorption efficiency, Q_{abs} of nanospheres and nanoshells with the bulk dielectric constants taken from Weaver and Frederikse, (Weaver & Frederikse, 2001) for nanospheres and nanoshells in vacuum. Besides, shell core were also embedded in vacuum.

Table 2.2: Shell geometries for optimized absorption with and without surface scattering (Arnold & Blaber, 2009).

Element	No surface scattering			With surface scattering		
	Q_{abs}	Outer radius (nm)	Inner radius (nm)	Q_{abs}	Outer radius (nm)	Inner radius (nm)
Ag	12.2	57.4	56.5	5.7	32.8	27.2
Au	19.9	29.2	27.7	7.3	42.2	37.5
Al	13.1	5.8	0.0	10.9	6.6	0.0
K	20.6	27.8	24.8	11.4	29.8	23.0
Na	22.8	35.0	30.7	13.7	36.0	27.2

From the Figure 2.3 (A), it can be observed that without the inclusion of surface scattering, K has the best absorption efficiency with a value of 22.8 at a wavelength of 1144 nm, which is closely trailed by Na and Au, later comes the Ag and Al respectively. All the metals show their absorption peak in the visible optical range with the exception from Al, having its absorption spectra in ultra-violet province. Similar trend is witnessed for the graphs in Figure 2.3 (B), where surface scattering effects are considered. However, all the materials absorption spectra are blue-shifted as a result of including surface scattering calculation. In addition, the absorption efficiency is also

reduced for all the materials as well. Thus, it can be concluded that the alkali metals (Na and K) are the best optical absorbers, while Al has the potential in shorter wavelengths.

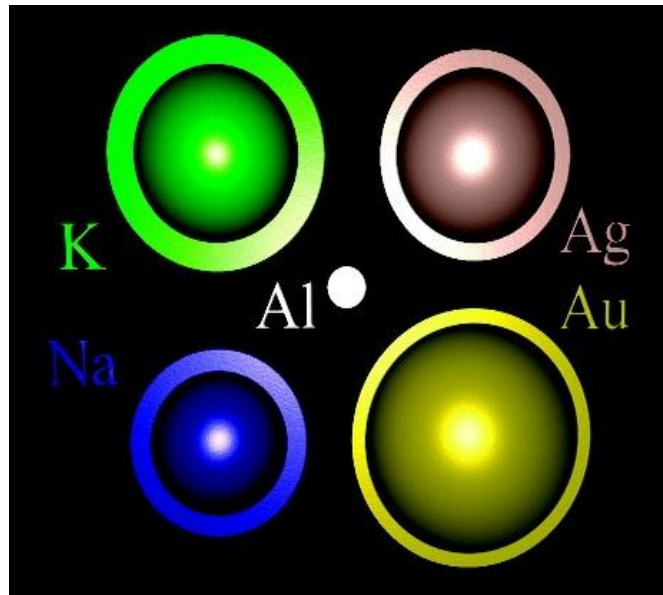


Figure 2.2: Optimized geometrical structure of the metals (Arnold & Blaber, 2009).

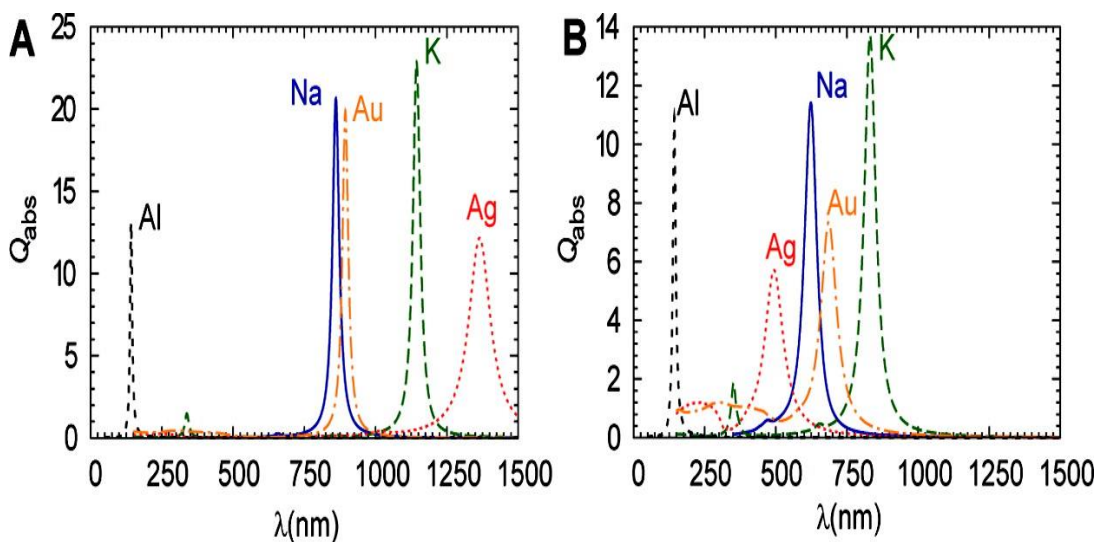


Figure 2.3: Optimized absorption spectra for nanoshells with radii and aspect ratios given in the Table 2.2 (A) without surface scattering and (B) with surface scattering (Arnold & Blaber, 2009)

In light of the discussions above, at this point, let us summarize the potential alternatives of silver and gold. On the basis of the above calculations, undoubtedly Na and K are the best plasmonic metals. However, both of these alkali metals are very much reactive to air and water. Thus, these metals are chemically unstable; hence their nanofabrication with controlled shape and size will be the toughest challenge. Nevertheless, they can still be used as in plasmonic applications either with proper coating techniques or, in such applications where they won't come into direct contact with oxygen or, water. But considering their extreme chemical instability, it should be quite expensive to fabricate and coat them in nano-scale. Therefore, there remains a big question-mark whether they can commercially compete with the likes of silver and gold! On the other hand, both of Cu and Al have satisfactory performance despite that they are not as good as other metals. But the advantageous part is both of these metals are cheaper and abundant in comparison with silver and gold. So, as conclusion, we can say that despite of showcasing excellent plasmonic quality, due to their chemical instability alkali metals do not seem to be a commercially competitive alternative of silver and gold. Al and Cu are not as good as silver and gold when the plasmonic quality is concerned. In such condition, one effective way to improve the plasmonic quality of the materials can be performed by shifting their interband transitions to another (less-important) part of the spectrum. This can be accomplished by alloying two or more metals to form distinctive band structures which can be fine-tuned by regulating the quantity of each alloyed metals. (Naik et al., 2014)

2.6. Bimetallic nano-alloys for potential plasmonic materials

Bimetallic nano-alloys, which are the aggregation of two types of metal atoms of nanoparticle size, have been utilized as key components in many catalytic, optical and

magnetic devices. It has been subject to an interest of both theoretical and experimental research for its distinct physical and chemical properties (Zhurkin et al., 2007) Now a days, there is a growing interest in bimetallic nanoparticles, compared to monometallic nanoparticles because bimetalization can offer space of improvement in optical, catalytic and magnetic performance over the original pure mono-metal nanoparticles and can create new properties. Also, molecular tuning of these bimetallic nanoclusters may give rise to novel properties which are not realized in bulk or, monometallic nanoparticles. (Ferrando et al., 2008; Rodriguez & Goodman, 1992)

As discussed in the previous section that both of Al and Cu are abundant on earth; hence inexpensive as well. However, their low plasmonic quality is the prime hindrance behind their commercial usage. Similarly, even though silver is the most popular plasmonic metal to date, their plasmonic performance is not up to the mark. On contrary, alkali metals despite of possessing the best plasmonic quality aren't used in plasmonic applications due to their extreme chemical instability. Thus, doping of alkali metals ($X = \text{Li, Na, K}$) into the Ag, Al and Cu metals to form Ag-X, Al-X and Cu-X nanoalloys can be a very effective solution for the search of alternative plasmonic materials.

Now, regarding the case of Ag-X nanoalloys, silver is a very expensive metal and alloying with alkali metals will make the fabrication process even more complicated. However, this alloying will substantially improve the plasmonic quality of the Ag-X nanoalloys with respect to bare silver nanoparticles; hence justifying the worth of alloying. Moreover, both silver and alkali metals have only s - valence electrons, hence making the system simple. Moreover, the large difference in electronegativity between Ag and alkali metals makes it favorable for mixing. Furthermore, the large gap for the cohesive energies and atomic radii between the silver and alkali metals favor the core-

shell segregation is another key reason for selecting the Ag-X bimetallic clusters as the model for computation (Fournier et al. 2009). Thus, elemental free electron metals (alkali metals) addition into the Ag nanocluster may potentially introduce some significant property-changes in the Silver nanocluster which will be an interesting study to explore. Similarly, the addition of alkali metals into the Cu and Al is expected to significantly improve the plasmonic response of the Al-X and Cu-X alloys compared to their stand-alone counterpart. In addition, reactive nature of both Al and Cu towards oxygen and water is another problems engineer and scientists have to face to fabricate them in nano-scale. The large Pauling electronegativity gap between the Al and Cu with the alkali metals will introduce some ionic bonding into the system. Thus, the alloyed Al-X and Cu-X compounds should be more stable than undoped Al and Cu; hence their reactivity towards water and air should be inferior as well. Moreover, both of the Cu and alkali metals have one -s electron in the outer shell; hence the Cu-X system should be simple to interpret. On the contrary, Al has one -p electron in their valence band which will result in s-p hybridization in the Al-X alloy; hence their electronic evolution will be an interesting story to study.

Research on Ag-X, Al-X and Cu-X nanoalloys are being reported in literatures. Let's consider the Ag-X alloys first. To date, several theoretical and experimental reports have been found on silver-alkali metals nanoalloys including Ag-Li alloy (Debnath & Said, 2014; Lee et al., 2010) and photoionization spectroscopy of metal dimers containing Ag-Li (Pilgrim & Duncan, 1995), Ag-Na (Stangassinger et al., 1997), Ag-K (Yeh, Robbins et al., 1993). In contrast, Al-Li alloys have been used as popular aerospace material for many years (Prasad et al., 2013) but their alloys are mostly in the bulk metal level. In nano-scale, both theoretical and experimental reports have been found on physical and chemical properties regarding Al-X (Ashman et al., 2002;

Khanna et al., 2002) and Cu-X (Fuentelba & Padilla-Campos, 2005; Li et al., 2015; Lin et al., 2006) bimetallic nanoparticles. Here it worth mentioning that all the reports mentioned above have discussed mostly the electronic and chemical properties of the alloyed materials and to our knowledge, this is the first research work where the optical absorption properties of the Ag-X, Cu-X and Al-X have been explored for very small nanoparticles such as 3 nm. The very next section will discuss our theoretical model for the Ag-X, Cu-X and Al-X nanoalloys.

2.7. 13-atoms icosahedral structures as the quantum model of Ag-X, Cu-X and Al-X nanoalloys

In the last few decades many reports have been found regarding the investigation of various noble-metal nano-clusters of different shapes such as rods, cubes, plates, icosahedra, decahedral, truncated octahedral and octahedral geometries. For our research, we have selected the 13-atoms and it is a well-known fact that icosahedral is at least a local minima for almost all the metals, if it is not a global minima. Now, Icosahedron with I_h symmetry is a platonic solid with 20 equilateral triangles as its faces and 5 such triangles meeting at each vertex can therefore be described as a model of larger multi-shell nanoparticles (Berry & Haberland, 1994). It had been observed that the metallic and bimetallic nanoparticles form highly symmetrical multi-shell structures with icosahedral, decahedral and cubo-octahedral symmetry. Furthermore, the 13-atoms cluster is the smallest core-shell structure (about 0.6 nm of diameter), with either icosahedral or, cubo-octahedral symmetry, which possesses a specific symmetry where a central atom is surrounded by 12-atoms closed shell (Moussab et al., 2010). Now, due to its special feature, core-shell structures carry special importance in Nano science. For example, core-shell nanoparticles are highly functional materials with modified

properties. In addition, as the shell material is used as the coating over the core-materials, it can provide control over the core-material properties. For instance, shell materials can be used effectively to decrease the chemical reactivity of the core-metal, which in turn gives the key to adjust the thermal stability. Moreover, the presence of shell-coating can provide assistance to control the parameters such as surface modification and dispensability as well. In our case, as we will be using highly reactive alkali metals as the doping element, shell-coating can be an excellent way to fine-tune the reactivity of the core-materials.

Interestingly, for bare Ag_{13} clusters, some DFT calculations (M. Harb et al., 2008; Yang et al., 2006) have shown that the most stable structure is an entirely deformed structure with $C1$ symmetry, which actually contradicts the findings of previous empirical studies that suggested the icosahedron structure as the lowest energy isomer. (Michaelian, Rendón, & Garzón, 1999) But several reports (Alamanova et al., 2007; Pereiro & Baldomir, 2007) have been found where it is clearly proven that Ag forms a highly stable structure at 13 atoms level with icosahedron symmetry. Thus, the core-shell 13-atom clusters can be considered as small enough to be treated with first-principles (DFT) methods, which can be considered as the quantum models for large nanoparticles for which such calculations cannot be done. (Harb et al., 2010)

Regarding the case of Cu_{13} clusters some DFT calculations have shown that the most stable structure is an entirely deformed structure with $C2$ symmetry, (Chou et al., 2013; Guvelioglu et al., 2005) which actually contradicts the findings of previous empirical studies that suggested the icosahedron structure as the lowest energy isomer. However, the Icosahedron 13-atom clusters are still stable even if not the global minima; hence can be considered as the quantum models for large nanoparticles for which such calculations cannot be done. (Harb et al., 2010) On the contrary, Al is reported to have

its global minima with icosahedral symmetry, although some literatures can also be found as well, where slightly distorted icosahedral with $d3d$ symmetry is described as the global minima. Now, whilst the electronic and optical properties of any material's nanoparticle changes with the change of the size, this quantum model will provide an indication of the trend of changes in electronic and optical properties as the result of doping alkali metals into Al and Cu clusters. For this reason, we have selected this 13-atoms structure (typically 3 nm in size) as the quantum model for those size and shaped particles for which such calculations cannot be done to predict the electronic, chemical and optical properties of the nano-alloys.

2.8. Summary

In consideration of above circumstances, it can be summarized as follows. Ag and Au have been the mostly used as conventional plasmonic materials even though these materials possess high interband and intraband transition losses. In addition, being noble metals both of them are reactive to air and oxygen; hence the fabrication process in nano-scale is difficult. Moreover, both of silver and gold are very expensive material, which is the main hindrance behind their commercial competitiveness. In such situation, looking at the alternative plasmonic materials, alkali metals (Li, Na, K) are found to show remarkable optical properties. In addition, Cu and Al also exhibit promising plasmonic qualities, though they are not as good as Ag, Au or, alkali metals. On the other hand, despite of having outstanding plasmonic properties, alkali metals still do not seem to be practically feasible option due to their high reactive nature towards oxygen and water.

In a separate note, bimetallic nano-alloys, which are the aggregation of two types of metal atoms of nanoparticle size, can be a solution to such problems. The major

advantage of bimetallic alloys is they can offer the plasmonic tuning by varying either the materials or, the quantity of the materials. Therefore, we have come with an idea of doping alkali metals into Ag, Al and Cu to form Ag-X, Al-X and Cu-X nano-alloys respectively in order to find the changes in electronic, chemical and optical properties it brings as a result of doping.

Now, with the intention of finding the electronic and optical properties of the bimetallic alloys mentioned above, 13-atoms icosahedron core-shell structure is selected as a quantum model of these metallic alloys. Now, it is a well-known fact that the metallic and bimetallic nanoparticles form highly symmetrical multi-shell structures with icosahedral symmetry. In addition, the most attractive feature of core-shell structures is the shell part will provide the coating here, which can be a very effective way to protect the alkali metals from the touch of oxygen and water. Therefore, we have selected this 13-atoms Icosahedron structure, which is roughly 3nm in size as the quantum model of the Ag-X, Al-X and Cu-X nanoalloys to find out whether these additions of alkali metals bring some positive changes in the alloyed metals compared to their undoped counterpart.

Here, in this chapter the current stage of plasmonic materials, merits and demerits of conventional materials have been discussed with theory as well. Later, we have checked the list of alternative plasmonic metals, which was followed by our proposed bimetallic alloys with proper reasoning. Finally, a 13-atoms core-shell structure with icosahedron symmetry is proposed as the theoretical quantum model for the Ag-X, Al-X and Cu-X nano-alloys in order to check whether this alloying has brought any positive changes in the chemical and optical properties of the alloyed metals. The very next chapter will comprehensively discuss the theoretical approach and methodology of the research done, which will be followed by the gained results and discussion chapter.

CHAPTER 3

RESEARCH METHODOLOGY

“I have a dream that my four children will one day live in a nation where they will not be judged by the color of their skin, but the content of the character.”

The above mentioned lines are taken from the famous speech named “I have a dream” of American civil rights activist, Martin Luther King Jr. It was August 28, 1963 when he delivered this speech in which he calls for an end to racism in the United States during the Washington DC Civil Rights march. Hundreds of years, people had been tortured only because they had black skin. In a separate window, let us look at this racist behavior from physics’ perspective. What we know from physics is, if a material reflects all the visible light, the material seems white and in contrary, if the material absorbs all the light, it appears black. Thus, when we are saying someone “black”, it is actually because he is covered by a polymer (human skin is just a polymer!) which absorbs all the visible light! And just because they had skins which absorb all the visible light, black people had to endure untellable torture for hundreds of years and I can just wish, if those idiot people knew some optical physics!!

Today, after 50 years of Martin Luther King’s famous speech when he fought for the rights of the people whose skins absorb all the visible light, I am presenting here my research methodology in order to find the optical properties of the proposed Ag-X, Al-X and Cu-X nano-alloys. In this chapter, the discussion will begin with the graphical representation of the theoretical model, which will be followed by explaining the functionals used in density functional theory.

3.1. 13-atoms core-shell structure of Ag-X, Al-X and Cu-X nano-alloys

In the previous chapter, the reasoning behind selecting these 13-atoms models has been explained with deliberation. Here, Figure 3.1 shows the icosahedral 13-atoms clusters of undoped Ag and the doping positions of alkali metals into pure Ag. As the doping methodology is very similar for all of Ag, Al and Cu, only Na doped Ag clusters is shown in the figure. Now for the doping, two positions are selected. First doping is shown in Figure 3.1(a), one Ag atom is replaced from the core of the Ag_{13} structure and is labeled as the core-doped (c-doped) Ag_{12}Na . The other doping is done by replacing one Ag atom from the shell of the Ag_{13} cluster, which is shown in Figure 3.1(b) and this structure is labeled as shell-doped (s-doped) Ag_{12}Na . Similar doping have been done for Al and Cu as well, where one Al and Cu atom have been replaced by X (X=Li, Na, K) atoms in the core and shell positions to form c-doped and s-doped Al_{12}X and Cu_{12}X clusters respectively. The geometrical, electronic, chemical properties of the bimetallic clusters will be explored which will be followed by the optical properties calculation in the later part of this work.

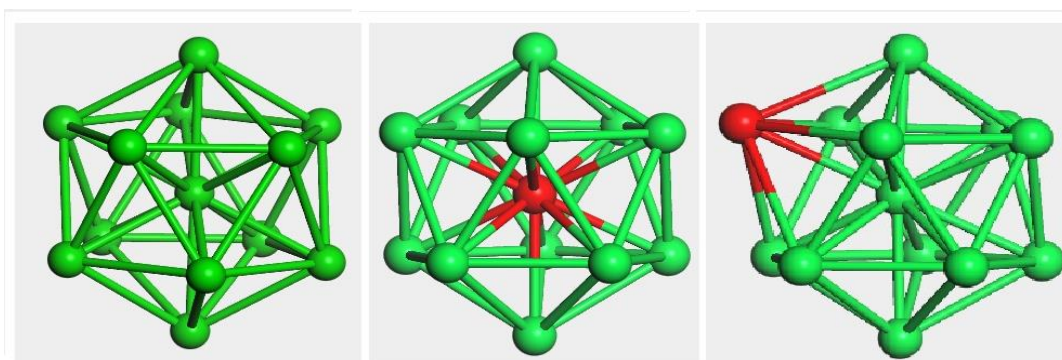


Figure 3.1 (a) Ag_{13} structure of icosahedral symmetry, (b) Na doped into the core, (c) Na-doped into the shell

3.2. Geometrical optimization and stability calculation

In our work, the primary focus is the optical properties of the bimetallic nano-alloys. But for any applications, before checking the optical properties, it is important to check the geometrical and structural stability of the doped clusters in order to ensure that the resultant bimetallic nano-alloys will practically sustain the structural stability.

3.2.1. Geometry optimization

To ensure the geometric stability, first of all the bimetallic clusters are geometrically optimized. The optimization of a structure is a two-step process:

- 1) **Energy evaluation:** The energy expression must be defined and evaluated for a given conformation. Energy expressions which include external restraining terms, to bias the optimization, may be defined in addition to the energy terms.
- 2) **Conformation adjustment:** The conformation is adjusted to reduce the value of the energy expression. A minimum may be found after one adjustment or may require many thousands of iterations, depending on the nature of the algorithm, the form of the energy expression, and the size of the structure.

The efficiency of the optimization is therefore judged by both the time needed to evaluate the energy expression and the number of structural adjustments (iterations) needed to converge to the minimum.

3.2.2. Harmonic vibrational frequency

Next, after the geometrical optimization is done, it is necessary to check whether the geometrically optimized structures are stable or, not. Harmonic vibrational frequencies

may be obtained from the matrix of Cartesian second derivatives, also known as the Hessian matrix, of a molecular or periodic system. (Wilson, Decius, & Cross, 1955)

For the case of molecule (or any finite system) the elements of the Hessian, H_{ij} , are given by the second derivative of the total energy E :

$$H_{ij} = \frac{\partial^2 E}{\partial q_i \partial q_j} \quad (3.1)$$

where q_i is a Cartesian coordinate of a system with N atoms, so that $1 < i < 3N$.

For the periodic case, there is an infinite number of atoms, but due to the periodicity ($H_{ij} = H_{i+T, j+T}$), the infinite Hessian matrix can be Fourier transformed into an infinite set of $3N \times 3N$ matrices, where N now stands for number of atoms in the unit cell.

$$H_{ij}^k = \frac{1}{V} \sum_T i.j + T e^{ihT} \quad (3.2)$$

Here, \mathbf{T} is the lattice translations vector and \mathbf{k} represents the vector in the first Brillouin zone.

For many phenomena, such as infrared spectra, for example, the most important factor is the Hessian matrix for the case where $\mathbf{k} = 0$, i.e., at the Γ -point. Thus, the Hessian for periodic systems will hereafter be referred to as the Hessian at the Γ -point.

The mass-weighted Hessian is obtained by dividing Hessian elements by the square roots of the atomic masses:

$$F_{ij} = \frac{H_{ij}}{\sqrt{m_i m_j}} \quad (3.3)$$

According to the harmonic approximation, the vibrational frequencies are the square roots of the eigenvalues of F and the normal modes are the eigenvectors of F .

Now, in order to check the stability of the geometrically optimized structures, absence of negative frequency ensure the structural stability of the clusters. Negative eigenvalues correspond to modes in which the energy is not a local minimum. Generally, these indicate that the system is in a transition state. The normal mode corresponding to this eigenvalue is the mode that moves the system in the direction of a local energy minimum. The frequencies obtained from negative eigenvalues are obviously imaginary numbers. However, by convention, such frequencies are given as real negative numbers.

3.2.3. Bond-length comparison

The comparison of the bond lengths between the pure atoms and doped atoms is an effective way to evaluate the structural stability. Typically, if the bond lengths of the doped clusters are found similar with the stable undoped one, the doped clusters are mostly stable as well.

3.3. Electronic and chemical stability calculation

The electronic and chemical stability of the nanomaterials must be ensured in order to make sure its long term stability in the targeted applications. In our calculation we will be measuring the following parameters to predict the electronic and chemical stability of the bimetallic nanoalloys.

Binding energy (BE) is the energy that must be exported from a system for the system to enter a bound state at a negative level of energy. Negative energy is called "potential

energy". A bound system is synergetic and thus has a lower (*i.e.*, more negative) potential energy than the sum of its parts—this is what keeps the system aggregated in accordance with the minimum total potential energy principle. Therefore, a system's binding energy is the system's synergy. For a cluster, the higher the binding energy, more stable is the cluster. Thus, high binding energy is a primary criterion for the selection of any nano-alloy. In our calculation binding energy (BE) of the clusters are measured using the following equation:

$$BE (Ag_{12}X) = 12E(Ag) + E(X) - E(Ag_{12}X) \quad (3.4)$$

HOMO-LUMO Gap is the energy difference between the HOMO and the LUMO, when HOMO and LUMO stand for Highest Occupied Molecular Orbital and Lowest Unoccupied Molecular Orbital respectively. HOMO and LUMO are sometimes referred to as frontier orbitals. The difference in energy between these two frontier orbitals can be used to predict the strength and stability of transition metal complexes, as well as the colors they produce in solution. (J.-Q. Chen, Ping, & Wang, 1989; Fuller, Davis, & Waychunas, 1993)

Now, it is well known that the magic-clusters with high symmetry and closer electronic shells have large HOMO-LUMO gaps; hence the clusters are generally stable and unreactive (Yildirim et al., 2011). But despite the immense utility of the MO theory, commonly used DFT functionals are seen not predicting the orbital energies accurately (G. Zhang & Musgrave, 2007). On the other hand, Koopman's theory recommends that at the Hatree-Fock (HF) level the eigen value of HOMO energy should be a good approximation to predict the negative experimental IP (Cramer, 2013). Similarly, the LUMO energy should be equal to the negative value of EA considering the assumption that the orbitals do not relax. But the reliability of the Koopman's theory for predicting

EA is question worthy due to its significant effect of orbital relaxation over the eigen value of LUMO energy (Garza et al., 2000). Therefore, the accuracy of a functional method is generally tested by comparing the HOMO energy and negative IP of the clusters. Among the DFT functionals, DJ Tozer and C.B. Musgrave et al (Tozer, 2003; Tozer & De Proft, 2005; G. Zhang & Musgrave, 2007) have reported that the orthodox GGA and LDA are continuum functionals; hence their predicted eigenvalues for HOMO are shifted upward by half of the integer discontinuity. On the contrary, Zhan et al (Zhan, Nichols, & Dixon, 2003) examined the HOMO eigenvalues along with HOMO-LUMO gap of some clusters with B3LYP functionals and found there exists linear correlation between the B3LYP predicted values with the corresponding experimental values. Thus, based on the above mentioned reports, we have used B3LYP functionals for calculating the HOMO-LUMO gaps of all the clusters considered in this whole work.

Ionization potential (IP) of an atom or molecule describes the minimum amount of energy required to remove an electron (to infinity) from the atom or molecule in the gaseous state. The units for ionization energy vary from discipline to discipline. In physics, the ionization energy is typically specified in electron volts (eV) and refers to the energy required to remove a single electron from a single atom or molecule. IP is generally of two types: a) Vertical ionization potential and b) adiabatic ionization potential. In times of calculating vertical ionization potential, it is let that the charged molecules have different geometry than the neutral ones. On the other hand, if the charged clusters maintain the same geometry of the neutral clusters, it is called vertical ionization potential. In our calculation, we will be using vertical ionization potential.

Electron Affinity (EA) of an atom or molecule defines as the amount of energy released when an electron is added to a neutral atom or molecule in the gaseous

state to form a negative ion. As like as the previous one, we will calculate the vertical electron affinity here. In our calculation, the IP and EA is calculated by the binding energy differences between the neutral clusters and the positively and negatively charged clusters respectively.

In the light of the above discussions, it can be summarized that the higher value of binding energy and HOMO-LUMO gap will offer more electronic stability of the nanoalloys, whereas the low the value of IP and EA, the more reactive will be the nanoalloys.

3.4. Optical absorption calculation

After discussing the structural, electronic and chemical stability, let's now focus our concentration towards the key parameter, which is the optical absorption of the nanoalloys. In recent years several theories have been implemented to study the optical spectra of nanoparticles and nanoclusters, such as Mie theory, (Mie, 1908) discrete dipole approximation (DDA) (Draine & Flatau, 1994), and electromagnetic finite difference time domain (FDTD) (Kunz & Luebbers, 1993). In recent times, time dependent density functional theory (TDDFT) (Marques et al., 2012) has been used to investigate the optical properties of noble metal clusters and the quantum mechanical TDDFT has been found to be satisfactory in unfolding small (less than 20 atoms) nanoclusters with detailed explanation of the electron extinction process. It has been reported in many literatures (Ma & Chen, 2012, 2013) that TDDFT calculations is satisfactory in explaining the relationships between SPR and the structure and size of pure noble metal nanoclusters of octahedral, cubic and icosahedral structure which encouraged us eventually to use TDDFT for calculating the optical spectrum.

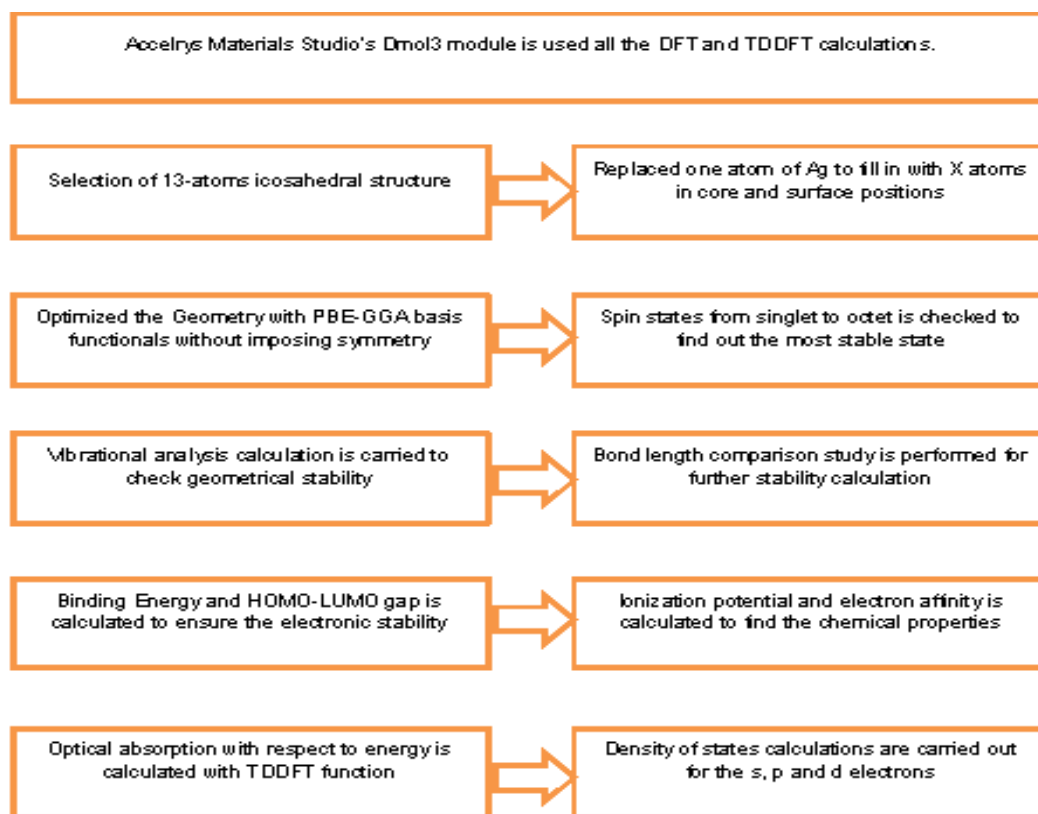
To predict the optical properties of the bimetallic clusters, we have calculated the oscillation strength of the clusters with respect to the energy in electron volts (eV). After that, we used a broadening method in order to provide a result easier to compare with the experiment. In experiment, spectra are generally made of bands or broad peaks. The peak width is due to the temperature effects, vibrations, uncertainties in measurement experiment, etc. The broadening we have made is an artificial way to take into account the broadening seen in experiment. If the experiment is made at low temperature and with “perfect” measurement devices, then the experimental spectrum will be similar to our stick spectrum. In evaluating the optical spectra of all the nanoalloys here, the Gaussian broadening is used for Ag-X clusters, whereas Lorentzian broadening is preferred for Cu-X and Al-X clusters. In addition, for Ag-X clusters we have used 50 steps calculation in singlet, whereas we did the calculation up to 500 and 1000 steps for Cu-X and Al-X clusters correspondingly. For silver, as their typical peak is in the range of 3.1-3.3 eV, up to 50 steps calculation was enough for that. But both of Cu and Al has their absorption peak in UV-Vis and UV region respectively. Thus, higher steps were required for them. After discussing the computational process of finding the structural and electronic properties of the clusters, which is followed by chemical and optical properties, the last section of this chapter will describe the computational method.

3.5. Computational method

In this study, we have used the density functional spin-polarized calculations using DMol3 of Accelrys Inc. code (Delley, 1990, 2000) to investigate the geometrical and energetic stabilities and optical properties of Ag₁₃, Al₁₃ and Cu₁₃ clusters with Icosahedral (Ih) symmetry and c-doped and s-doped Ag₁₂X, Al₁₂X and Cu₁₂X bimetallic

structures. All geometrical structures of the neutral clusters are optimized without imposing symmetry. Calculations have been performed using the Perdew-Burke-Ernzerhof (PBE) exchange-correlation functional. (Perdew, Burke, & Ernzerhof, 1996) The Kohn-Sham equation was expanded in a double numeric quality basis set (DNP) with polarization functions. To consider the relativistic effect, the DFT Semi-core Pseudo-potentials (Delley, 2002) are used for the treatment of the core electrons of the doped clusters. The orbital cut off range and Fermi smearing were selected as 5.0 \AA^0 and 0.001 Ha respectively. The self-consistent-field (SCF) procedures were performed with the aim of obtaining well converged geometrical and electronic structures with a convergence criterion of 10^{-6} a.u. The energy, maximum force and maximum displacement convergence were set as 10^{-6} Ha , 0.002 Ha/\AA^0 and 0.005 \AA^0 respectively. The cationic and anionic structures are also optimized by GGA-PBE energy calculation with same functionals basis set and keeping the same symmetry of neutral structures for computing the values of Ionization Potential (IP) and Electron Affinity (EA). B3LYP functionals are used to calculate the HOMO-LUMO gap of the optimized neutral clusters. The ALDA kernel exchange co-relation method was employed with TDDFT for calculating the optical excitation spectra. (Gross & Kohn, 1990) In addition, Gaussian broadening is applied to the eigen values here to get the optical spectra of the clusters. The vibrational analysis is also carried out to check the stability of the clusters, where absence of negative eigen value ensure the cluster stability.

At this point, to summarize the total computational method step by step, the algorithm of the computational process is presented below:



In this chapter we have comprehensively discussed the computational method we used in our research. In addition, background theory of the measured chemical and optical properties is added with the purpose of justifying the inevitability of those above mentioned properties. Thus, from here we will now move to the next chapter where the results of the computations will be analyzed with the aim of testing the potential of the Ag-X, Al-X and Cu-X nanoalloys for potential applications in opto-electronics and catalysis.

CHAPTER 4

RESULTS AND ANALYSIS

I lost my respect to Angstroms!

This line is taken from the autobiography of famous Noble Prize winning physicist Heinrich Rohrer. It was 1981 when the world observed the most important invention in the history of nanotechnology, the scanning tunneling microscope (STM) which came through the hands of Nobel Prize winning physicists Gerd Binnig and Heinrich Rohrer. After the invention of STM, finally the world was able to see the images of materials' surfaces in nano-level which is even smaller than angstrom and there comes the above-mentioned dialogues on angstroms! Thus the invention of STM allowed the scientists to observe the very interesting changes in materials properties in nano-scale compared to their bulk-sizes, and there practically started the actual history of nano-science.

Well, now let me tell something more interesting! Will you believe me if I say nanoparticles were used even 1600 years ago? There is a 1600-year-old Roman chalice at the British Museum which appears jade green when lit from the front but blood-red when lit from behind. This strange property of the chalice had puzzled scientists for decades after the museum acquired the cup in the 1950s. The mystery wasn't solved until 1990, when researchers in England scrutinized broken fragments under a microscope and discovered that the Roman artisans had impregnated the glass with particles of silver and gold which are 50 nanometers in size! Although the Romans were able to make and use nanoparticles for beautiful arts, most probably they never realized the true importance of nanoparticles. Here, after long 1600 years later, I am presenting my calculated results of electronic, chemical and optical properties of Ag-X, Al-X and

Cu-X nanoalloys but unlike the ancient Romans, now we all know the huge importance of nanoparticles!

This chapter is divided into four (04) sub-sections. For the case of Ag_{12}X alloys, we have looked at the properties of the alloyed nanoparticles of both of the icosahedron and decahedron shape, which is represented in first two sections of this chapter. The later section has comprehensively discussed the chemical and optical properties of Cu-X and Al-X nanoalloys, which will be followed by an overall summary.

4.1. Structural stability and the electronic, chemical and optical properties of 13-atoms icosahedral Ag_{12}X structures

The ground state of all clusters was determined by checking their total energy and binding energy with different spin multiplicity from singlet to octet. It was found that for Ag_{13} and all the doped clusters, the spin-5 (five) offers the most stable structures, which also confirms the findings of the previous reports (Harb et al., 2010; Ma & Chen, 2012; Rao et al., 2013) All the c-doped and s-doped Ag_{12}X neutral and charged clusters are geometrically optimized without imposing symmetry by nonlocal functional Generalized Gradient Approximation (GGA) with PBE as exchange function and DNP as basis set. Confirmation of the choice of functional and basis set were carried out by comparing the average bond length and vertical ionization potential (VIP) of the Ag_{13} cluster which we obtained with previous reports. M. Pereiro et al (Pereiro & Baldomir, 2007) have reported the average bond length and vertical IP of icosahedral Ag_{13} as 2.87 \AA and 6.34 eV (experimental) respectively, which are similar to our findings of average bond lengths and vertical IP of 2.8718 \AA and 6.65 eV respectively.

4.1.1. Geometrical structure and energetic stability

The optimized structures of Ag_{12}X clusters based on the icosahedral geometry of Ag_{13} are shown in the Figure 4.1. We note here that all the structures are optimized without imposing symmetry and to this end; we can see that c-doped structures maintained the Icosahedral (Ih) symmetry after optimization with the exception of c-doped Ag_{12}Rb , Ag_{12}Cs and Ag_{12}Fr clusters. The fore-mentioned three (3) clusters are reformed to C_1 , C_i and C_1 symmetry respectively after optimization. On the other hand, all the s-doped clusters possess C_{5v} symmetry. Now, to verify, whether the optimized clusters are stable or, not, we have calculated harmonic vibrational frequencies for all the clusters shown in the Figure-4.1. The stability of the clusters are confirmed by the absence of imaginary frequencies and in our calculation, except for the c-doped Ag_{12}Cs and Ag_{12}Fr , we haven't witnessed any imaginary vibrational frequency for any of the optimized clusters. Regarding the case of fore-mentioned clusters instability, most probably these two structures are still in the excited state rather than ground state, which result some imaginary vibrational frequency. The highest and lowest vibrational frequency of parent Ag_{13} and the doped clusters are charted in Table-4.1.

To further study regarding the geometrical structure of the c-doped and s-doped Ag_{12}X clusters, we have calculated the average bond lengths of Ag-X atoms as compiled in Table-4.2. Now, Table-4.2 clearly reveals that among all the c-doped and s-doped compounds, only Ag-Li bond distances are slightly reduced, while the Ag-Na bond length is similar to the corresponding Ag-Ag bond length. For the rest of the c-doped and s-doped compounds, Ag-X bond lengths are found larger than the corresponding Ag-Ag bond distance. Furthermore, Rb, Cs and Fr atoms doped clusters exhibit the highest deformation with respect to Ag_{13} cluster, implying the fact that these c-doped and s-doped Ag_{12}Rb , Ag_{12}Cs and Ag_{12}Fr are expected to be the least stable amongst all

the doped clusters considered here. On the other hand as we see that the Li and Na doped clusters result the least distortion from the undoped Ag_{13} cluster, thus, geometrically these c-doped and s-doped Ag_{12}Li and Ag_{12}Na clusters are supposed to be more stable compared to the other Ag_{12}X clusters.

Now focusing on geometric structures from the Figure-4.1, it can be observed that among all the Ag_{12}X clusters, Li and Na doping has produced the minimum amount of geometrical deformation, whereas from K atom onward we observe more deformation from the icosahedral structure, in both of the c-doped and s-doped structures. This deforming trend can be easily explained considering the fact that the atomic radii of the doped alkali atoms increases from Li (1.52 \AA) to Fr (2.82 \AA), while it maintains an incremental trend (Na: 1.54 \AA , K: 2.27 \AA , Rb: 2.48 \AA , Cs: 2.65 \AA) down the periodic table group. Besides, all these atomic radii are larger than the atomic radii of Ag (1.44 \AA). Thus, when we are doping similar sized atoms (let's say Li and Na) into Ag_{13} , it produces the minimum deformation compared to the parent Ag_{13} . Similarly, adding larger atoms results with higher geometrical deformation. Moreover, for the c-doped Ag_{12}Rb , Ag_{12}Cs , Ag_{12}Fr the optimized structures reforms to C1, Ci and C1 symmetries respectively, as the atomic radii of these atoms are too big compared to Ag to maintain a core-shell icosahedral (Ih) structure.

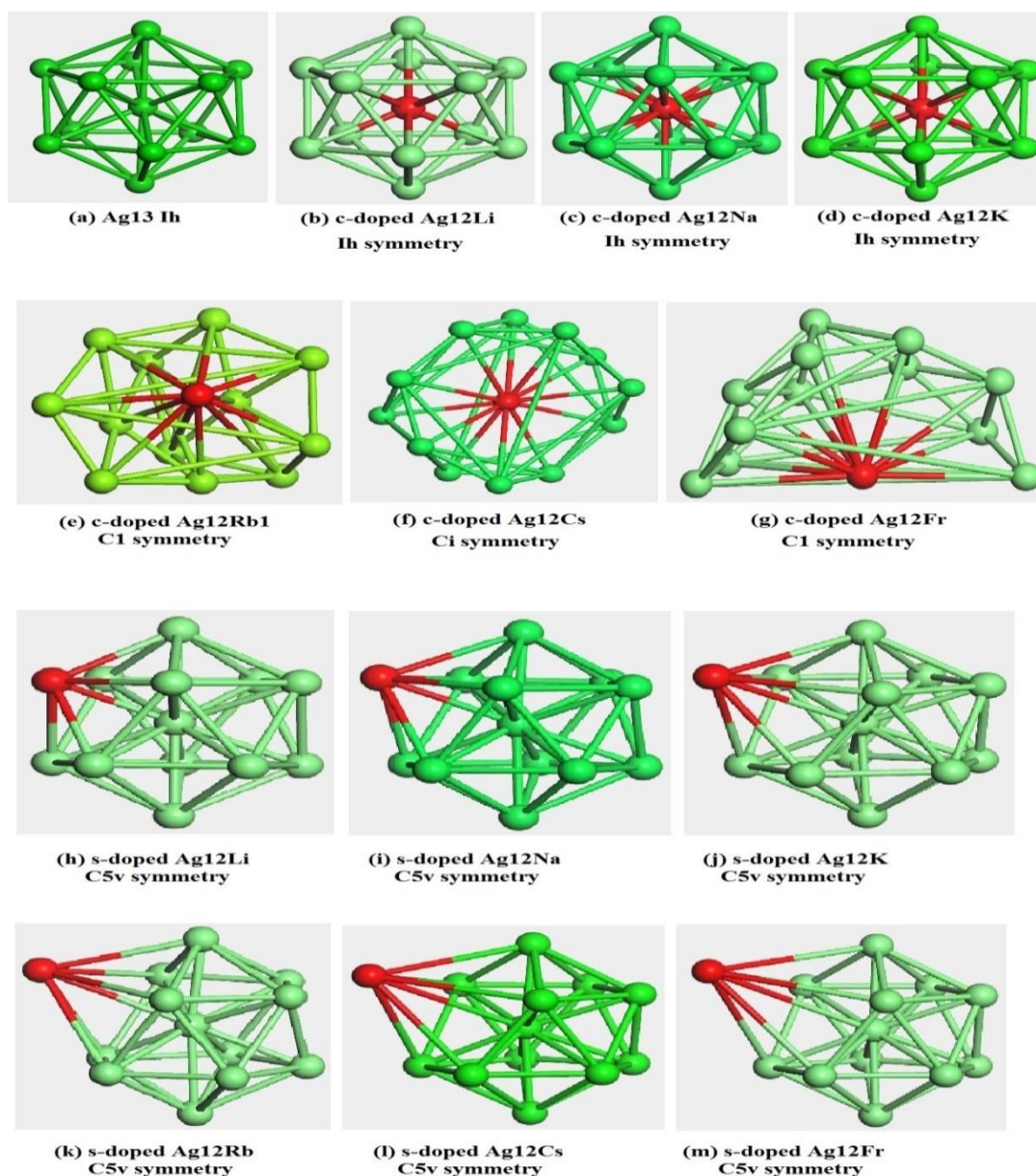


Figure 4.1: Optimized geometry of the icosahedral Ag_{13} and Ag_{12}X clusters

After discussing the outcomes of the geometrical structures of the Ag_{12}X bimetallic clusters and their degree of deformation from the parent Ag_{13} Icosahedral shape, now we move our focus to the thermodynamic stability of the doped clusters. For this, Table-4.3 and 4.4 are assembled with the data of entropy, enthalpy, heat capacity and the free energy of the clusters. The thermodynamic data of the c-doped Ag_{12}Cs and Ag_{12}Fr are

excluded from table as the fore-mentioned clusters are found unstable through vibrational frequency analysis. Here it worth mentioning that, all the thermodynamic properties is calculated at 25⁰ C.

Table-4.1: Vibrational frequency of the icosahedral Ag₁₃ and Ag₁₂X clusters

Compound	c-doped Ag ₁₂ X clusters		s-doped Ag ₁₂ X clusters	
	Lowest Vibration Frequency cm ⁻¹	Highest Vibration Frequency cm ⁻¹	Lowest Vibration Frequency cm ⁻¹	Highest Vibration Frequency cm ⁻¹
Ag ₁₃	50.93	179.75		
Ag ₁₂ Li	80.94	397.49	40.36	284.58
Ag ₁₂ Na	85.69	267.21	43.36	184.86
Ag ₁₂ K	44.50	262.70	42.43	186.36
Ag ₁₂ Rb	23.63	175.32	37.68	187.51
Ag ₁₂ Cs	- 31.80	154.20	29.82	183.07
Ag ₁₂ Fr	- 15.51	166.22	15.55	184.51

Table 4.2: Comparison of average Ag-X bond length of the nanoalloys

c-doped Structures	Average Bond Lengths (Å)	s-doped Structures	Average Bond Lengths (Å)
Ag-Ag	2.7998	Ag-Ag	2.9218
Ag-Li	2.7294	Ag-Li	2.8792
Ag-Na	2.7945	Ag-Na	3.1793
Ag-K	2.9009	Ag-K	3.5764
Ag-Rb	4.2084	Ag-Rb	3.7359
Ag-Cs	3.6508	Ag-Cs	4.0386
Ag-Fr	4.1179	Ag-Fr	4.3558

Table 4.3: Thermodynamic properties of c-doped Ag₁₂X clusters

Cluster	Entropy S Cal/mol.K	Heat Capacity H Cal/mol.K	Enthalpy H kCal/mol	Free Energy G kCal/mol
Ag₁₃	205.23	72.31	22.29	- 40.09
Ag₁₂Li	197.11	71.09	22.72	- 36.05
Ag₁₂Na	206.82	71.90	22.42	- 39.24
Ag₁₂K	225.17	72.30	22.29	- 44.84
Ag₁₂Rb	218.52	72.38	22.27	- 42.88

Table 4.4: Thermodynamic properties of s-doped Ag₁₂X clusters

Cluster	Entropy S Cal/mol.K	Heat Capacity H Cal/mol.K	Enthalpy H kCal/mol	Free Energy G kCal/mol
Ag₁₂Li	205.06	71.94	22.41	- 38.73
Ag₁₂Na	208.24	72.28	22.29	- 39.79
Ag₁₂K	210.44	72.34	22.28	- 40.46
Ag₁₂Rb	212.79	72.36	22.27	- 41.17
Ag₁₂Cs	216.15	72.41	22.26	- 42.19
Ag₁₂Fr	221.38	72.45	22.25	- 43.76

Now, from Tables 4.3 and 4.4, it can be clearly seen that with respect to Ag₁₃, the entropy increases for all the compounds except the c-doped Ag₁₂Li, implying the fact that the randomness of the system increases for all the doped clusters expect for c-doped Ag₁₂Li. Furthermore, we observe very small change in enthalpy and heat capacity of all the c-doped and s-doped Ag₁₂X clusters with respect to the parent Ag₁₃ cluster, yielding the fact that regarding the internal energy and response towards heat energy, the doped

clusters react similarly compared to pure Ag_{13} cluster. On the other hand, free energy can be described as the thermodynamic potential that measures the energy of the system can be converted to work; hence can be analogous to the potential energy of a closed system. Now, from the results of Tables 4.3 and 4.4, it is evident that the c-doped and s-doped Ag_{12}Li clusters exhibit highest free energy among all the clusters, and that is higher than the corresponding value of Ag_{13} clusters. Therefore, it is revealing the fact that in a specific temperature, more process initiating work is obtainable from the Ag_{12}Li clusters than the Ag_{13} or, any other clusters considered in this thesis.

4.1.2. Electronic Properties

After discussing the geometrical structure and stability of the doped clusters in the previous section, now we focus our attention towards the electronic structure of these doped clusters and for that Tables 4.5 and 4.6 are compiled with the binding energy (BE), vertical ionization potential (VIP), vertical electron affinity (VEA) and HOMO-LUMO gap of the entire c-doped and s-doped Ag_{12}X clusters. As the vibrational analysis predicted that the c-doped Ag_{12}Cs and Ag_{12}Fr clusters are not stable, we have excluded these clusters from the discussion on electronic and optical properties.

Observing the data of Tables 4.5 and 4.6, it can be clearly found that among the entire c-doped and s-doped structures only Ag_{12}Li has higher BE than the corresponding value of Ag_{13} . In particular, the c-doped Ag_{12}Li exhibits the highest BE amongst all the clusters deliberated here. We also observe that the s-doped Ag_{12}X clusters displays higher BE compared to c-doped Ag_{12}X compounds, signifying that the favored structure is c-doped Ag_{12}Li and the entire s-doped Ag_{12}X structures. The reason for this is, the bulk interatomic distances for Ag, Li, Na, K, Rb, and Cs, are 2.89, 3.023, 3.659, 4.525, 4.837 and 5.235 Angstroms, respectively. (Kittel, 2005) Thus, the strain for c-doped

Ag_{12}X_1 increases in the order $\text{X}=\text{Li}, \text{Na}, \text{K}, \text{Rb}, \text{Cs}, \text{Fr}$ and is very large for the biggest atoms. Therefore, they prefer the surface doping (s-doped) site. But interestingly, c-doped Ag_{12}Li has higher binding energy than Ag_{13} . We next focus our attention to the three more important indicators which are very crucial to characterize the chemical stability of small clusters, which are ionization potential (IP), electron affinity (EA) and HOMO-LUMO gap.

Tables 5 and 6 show that c-doped Ag_{12}Li has the highest VIP amongst all the structures considered. In addition, it is the only compound which exhibits higher VIP than Ag_{13} . Thus, it is obvious that except c-doped Ag_{12}Li , all the other doped Ag_{12}X clusters are expected to lose some electrons more easily than Ag_{13} cluster. On the other hand, all the doped Ag_{12}X clusters have shown lower VEA values with respect to Ag_{13} , yielding the fact that the doped clusters hang more easily with electrons compared to the parent Ag_{13} . Moreover, surprisingly c-doped Ag_{12}Rb cluster has displayed very low VEA (0.28 eV) compared to all the other clusters. Most probably, its change of symmetry from I_h to C_1 is the reason for their out-of-trend data of VEA.

Now if we focus our attention to the trend the doped clusters VIP and VEA are following, it can clearly be seen that the entire c-doped and s-doped Ag_{12}X clusters follow a decreasing trend from Ag_{12}Li to Ag_{12}Cs . The most probable reason behind this is due to the fact that the IP and EA of the Group – IA alkali atoms decrease periodically from Li to Cs down the group. Thus, when these alkali metals are doped into the Ag_{13} cluster, the doped Ag_{12}X clusters are expected to follow the same decreasing trend regarding their VIP and VEA values. Interestingly, the VIP and VE of s-doped Ag_{12}Fr are higher than Ag_{12}Cs , which can be well explained by the relativistic effect. (Thayer, 2010)

Table 4.5: Binding energy (BE), vertical ionization potential (VIP), vertical electron affinity (VEA) and HOMO-LUMO gap of the undoped icosahedral Ag₁₃ and c-doped Ag₁₂X bimetallic clusters

Cluster	Symmetry	Spin	BE (eV)	VIP (eV)	VEA (eV)	HOMO-LUMO Gap (eV)
Ag ₁₃	Ih	5	19.42	6.65	1.90	1.20
Ag ₁₂ Li	Ih	5	20.27	6.71	1.63	1.20
Ag ₁₂ Na	Ih	5	18.67	6.66	1.62	1.19
Ag ₁₂ K	Ih	5	16.53	6.32	1.58	1.15
Ag ₁₂ Rb	C1	5	18.48	5.32	0.28	0.35

Table 4.6: Binding energy (BE), vertical ionization potential (VIP), vertical electron affinity (VEA) and HOMO-LUMO gap of the s-doped Ag₁₂X bimetallic clusters

Cluster	Symmetry	Spin	BE (eV)	VIP (eV)	VEA (eV)	HOMO-LUMO Gap (eV)
Ag ₁₂ Li	C _{5v}	5	19.50	6.23	1.86	0.69
Ag ₁₂ Na	C _{5v}	5	19.08	6.13	1.73	0.73
Ag ₁₂ K	C _{5v}	5	19.20	5.82	1.65	0.58
Ag ₁₂ Rb	C _{5v}	5	19.18	6.03	1.61	0.55
Ag ₁₂ K	Ih	5	16.53	6.32	1.58	1.15
Ag ₁₂ Rb	C1	5	18.48	5.32	0.28	0.35

Apart from the BE, VIP and VEA, the energy gap between the HOMO and LUMO is considered as an important quantity for evaluating the electronic stability of clusters. In fact, it is well known that the magic-clusters with high symmetry and closer electronic

shells have large HOMO-LUMO gaps; hence the clusters are generally stable and unreactive (Yildirim et al., 2011). Now, from the data of Tables 5 and 6, it is clear that B3LYP predicted quite high values of HOMO-LUMO gaps for undoped Ag_{13} and c-doped Ag_{12}Li , Ag_{12}Na and Ag_{12}K clusters. Therefore, the fore-mentioned c-doped clusters are expected to be highly stable and non-reactive. In addition, the c-doped Ag_{12}Rb exhibit comparatively lower HOMO-LUMO gaps, where its change of symmetry is the most probable reason behind this. On the contrary, all the s-doped clusters show comparatively lower HOMO-LUMO gaps than the corresponding value of parent Ag_{13} . Here, it needs to be noted that, both Ag and alkali atoms have one valence electron, so these 13-atoms structures are 13 electrons system forms a kind of delocalized s-band system; (de Heer, 1993) which should be able to explain the comparatively lower HOMO-LUMO gaps of the s-doped bimetallic clusters.

After discussing the electronic properties of all the doped clusters considered, it can be concluded that the Ag_{12}X clusters follow a decreasing trend of BE, VIP and VEA from top to down the group. In addition, except Ag_{12}Li , all the other bimetallic clusters exhibits lower BE, VIP and VEA with respect to the parent Ag_{13} , yielding the fact that these doped Ag_{12}X clusters are electronically more active compared to pure Ag_{13} . On the other hand, it is reported that neutrals clusters with high HOMO-LUMO gaps are expected to be very active as anions because of their lower values of VEA (Molina & Hammer, 2005). Now, with the results presented in Tables 4.5 and 4.6, it is shown that neutral Ag_{12}Li and Ag_{12}Na clusters possess high BE and HOMO-LUMO gaps along with low VEA. Therefore, anions of these clusters are expected to be highly reactive compared to the corresponding of undoped Ag_{13} .

4.1.3. Optical absorption spectra

The absorption spectra of the Ag_{13} clusters are shown in the Figure 4.2 (a), where we have used TDDFT with ALDA kernel exchange-correlation terms in singlet state to calculate the spectra. For Ag_{13} , the main transition is found at 3.22 eV (Figure 4.2a), which is similar to the previous experimental reports (Weissker & Mottet, 2011) (Ma & Chen, 2012), thus confirming the justification of our theoretical method. Figure 4.2b and Figure 4.2c show the optical spectra of c-doped and s-doped Ag_{12}X clusters respectively. Now from the figures, it can be clearly observed that the c-doped Ag_{12}Rb of C_1 symmetry is the only compound among the entire c-doped and s-doped clusters, which is blue shifted with respect to the corresponding of the parent Ag_{13} , with optical peak at 3.33 eV. But the optical peaks of all the other c-doped and s-doped Ag_{12}X clusters are red-shifted compared to undoped Ag_{13} . It is reported that the increment of cluster size in a pure metallic nanoparticle system results to red-shift in optical bands (M. Harb et al., 2008; Cai et al., 2009), whereas except c-doped Ag_{12}Rb , all of our doped compounds optical peaks are red-shifted.

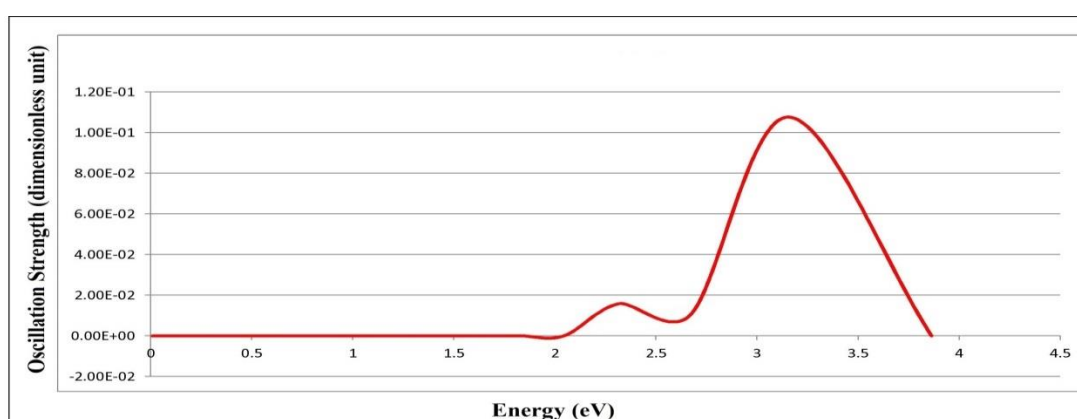


Figure 4.2(a): Optical absorption spectra of icosahedral Ag_{13}

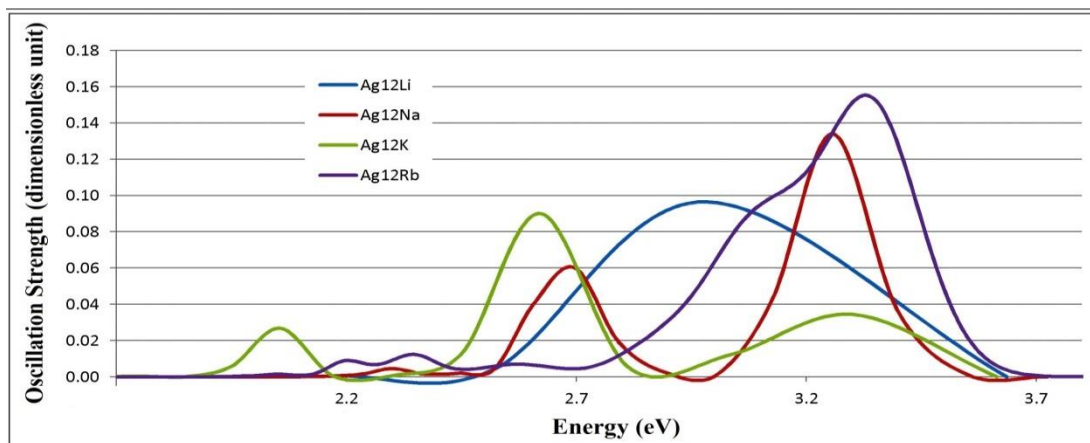


Figure 4.2(b): Optical spectra of c-doped $Ag_{12}X$ nanoalloys

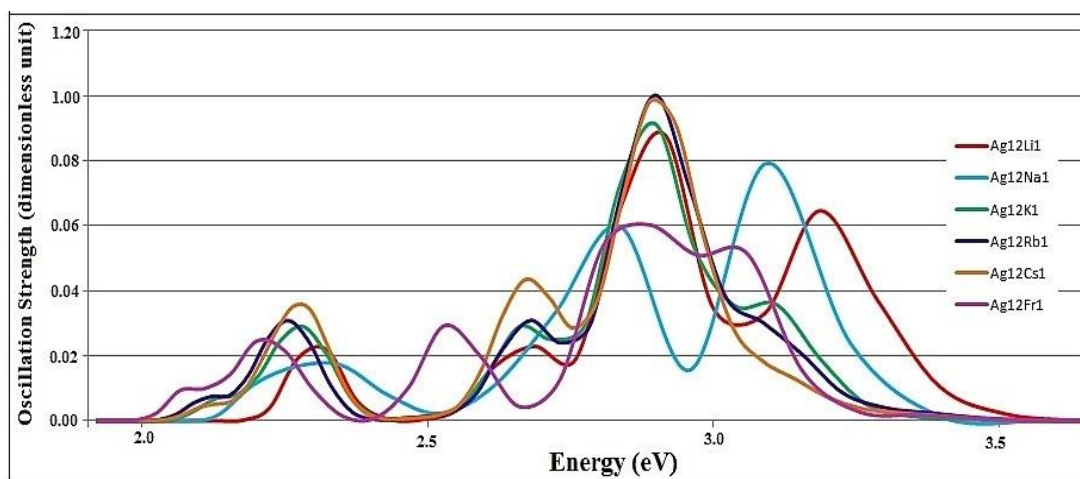


Figure 4.2(c): Optical spectra of s-doped $Ag_{12}X$ nanoalloys

Now let's move our focus towards the electronic evolution of the spectra of the doped clusters. Here, with the presence of alkali atoms these bimetallic $Ag_{12}X$ clusters in the excited states lead to a quasi-continuum spectrum. In particular, for the case of Ag_{13} , the electronic transitions are happening as a result of excitations from the s and d orbitals. These s and d orbitals are well localized in surface silver atoms, along with its evolution as hybrid s-p orbitals in the wide areas of outer region where several atoms are involved with the system (Harb et al., 2010). On the contrary, the absorption spectra of alkali metal clusters are explained as collective oscillation of *s valence electrons* and the shift

of absorption energies of very small particles, compared to the larger ones explained by a spill out (extension of the electronic wave functions out of the “classical volume” of the cluster) of these *s-electrons* (Harb et al., 2008). Therefore, when we are doping an alkali metal into the noble metal cluster, a systematic investigation of the excitations in molecular level is quite complicated. To this end, for investigating the absorption spectrum of the clusters we have presented the partial density of states (PDOS) calculation in Figure 4.3, where the PDOS of Ag₁₃, c-doped Ag₁₂Li and s-doped Ag₁₂Li are displayed.

Now, from the PDOS of Figure 4.3 (a-c), it is clearly observed that the actions of d orbitals in Ag₁₃ are more dominant in the in the energy range of -3 to 6.5 eV, with its peak at -3.2 eV. Now, in the cases of c-doped Ag₁₂Li and s-doped Ag₁₂Li, we find that the d electrons still exhibit the stronger role, but their peaks are red-shifted to -4.6 and -3.5 eV respectively, which indicates that d electrons are transferred to higher energy level for the doped clusters. Actually the doping of Li into the Ag nanoparticles results an increase in the occupation of empty s and p bands of the Ag₁₃ cluster, which eventually causes the d electrons transferred to higher energy level. Thus, this transfer of d electrons might well-explain the red-shifting of optical spectra of the doped Ag₁₂X clusters.

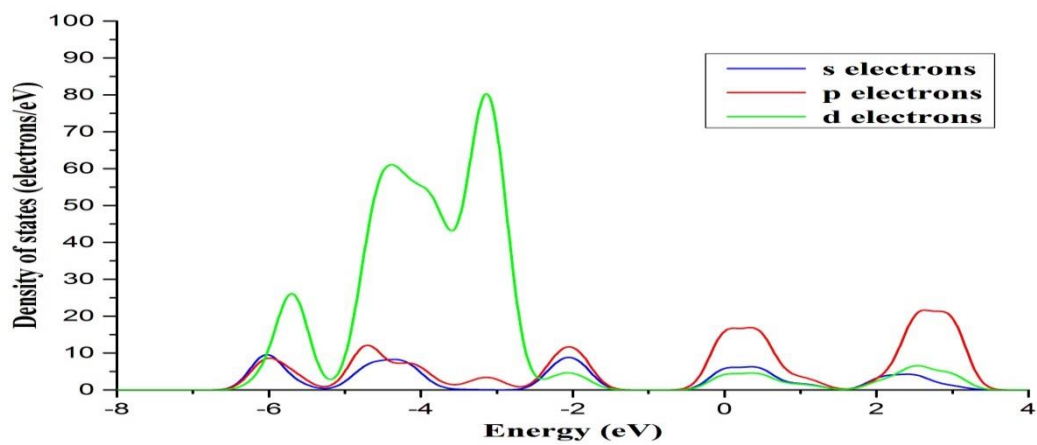


Figure 4.3(a): PDOS of Ag_{13}

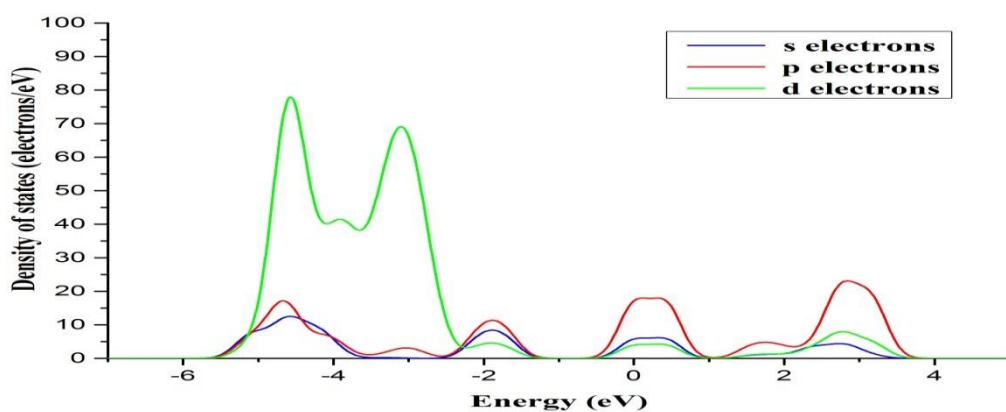


Figure 4.3(b): PDOS of c-doped Ag_{12}Li

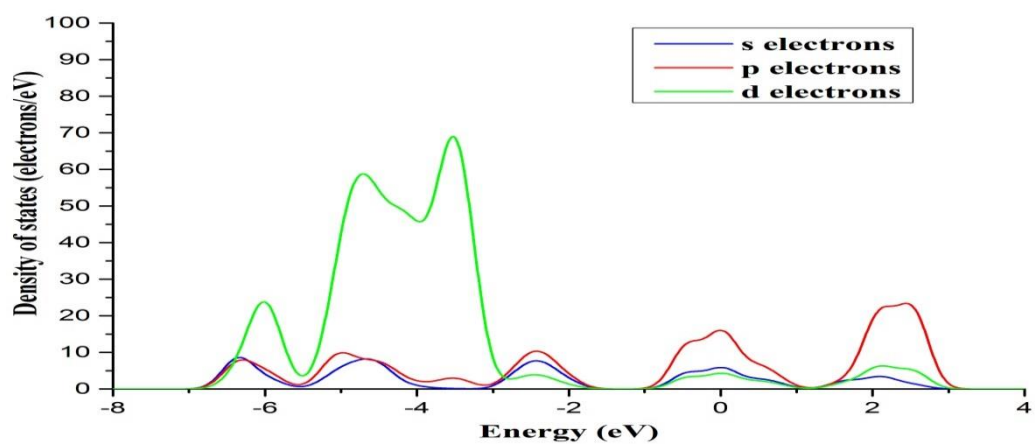


Figure 4.3(b): PDOS of s-doped Ag_{12}Li

4.2. Structural stability and the electronic, chemical and optical properties of 13-atoms decahedral Ag₁₂X structures

In this work, we have selected 13-atoms decahedral shaped Ag clusters to be doped by the alkali metals (X= Li, Na, K, Rb, Cs, Fr) in core, surface and vertex positions, which will be referred to c-doped, s-doped and v-doped Ag₁₂X bimetallic clusters respectively. Recent DFT calculations (Harb et al., 2008; Yang et al., 2006) have shown that the most stable structure is an entirely deformed structure with C1 symmetry which actually contradicts the findings of previous empirical studies that suggested the icosahedron structure as the lowest energy isomer (Michaelian et al., 1999). Thus, decahedral shaped Ag in 13-atoms level is not actually the global minima. Decahedral Ag in the size range of 35-120 nm has been established as a commercially available product for use in various opto-electronic, catalytic and biological applications. Thus this work explores the potential improvement of the Ag clusters properties through doping of alkali atoms into Ag. Therefore, as a first investigation, our 13-atom decahedral Ag₁₂X bimetallic clusters can be treated as the quantum models for the Ag-X bimetallic clusters (Harb et al., 2010). Whilst the electronic and optical properties of any material's nanoparticle changes with the change of the size, this quantum model will provide an indication of the trend of changes in electronic and optical properties as the result of doping alkali metals into decahedral silver.

4.2.1. Geometrical optimization and energetic stability

The ground state of all clusters were determined by checking their total energy and binding energy with different spin multiplicity from Singlet to Octet and it was found that for Ag₁₃ and all the doped clusters, the spin-1 (one) offers the most stable structures, which also confirms the findings of the previous reports. (Ma & Chen, 2012,

2013; Y. Rao et al., 2013) Given that the objective of this work is to predict the trend of change in electronic and optical properties in decahedral silver as the result of alkali atoms doping, all the calculations were carried out by imposing symmetry constraints so that the doped Ag_{12}X clusters maintain the similar or, at least adjacent symmetry of parent Ag_{13} cluster of D_{5h} symmetry.

Figure 4.4 shows the optimized structures of the doped Ag_{12}X clusters. Along with center doping (c-doping), surface doping has been done in two positions; one in the vertex and the other one in the shell, which will be calling v-doped and s-doped clusters from now on. Now, from the Figure-4.4, it is evident that all the c-doped clusters maintain the same D_{5h} symmetry of the parent Ag_{13} , whereas the v-doped and s-doped clusters reform to C_{5v} and C_s symmetry respectively. To this end, examination of the geometric degree of deviation of the doped bimetallic clusters compared to parent Ag_{13} has been a focus of investigation and towards that end the calculation for the average Ag-X bond lengths of the entire Ag_{12}X clusters and compiled those data in Table-4.7.

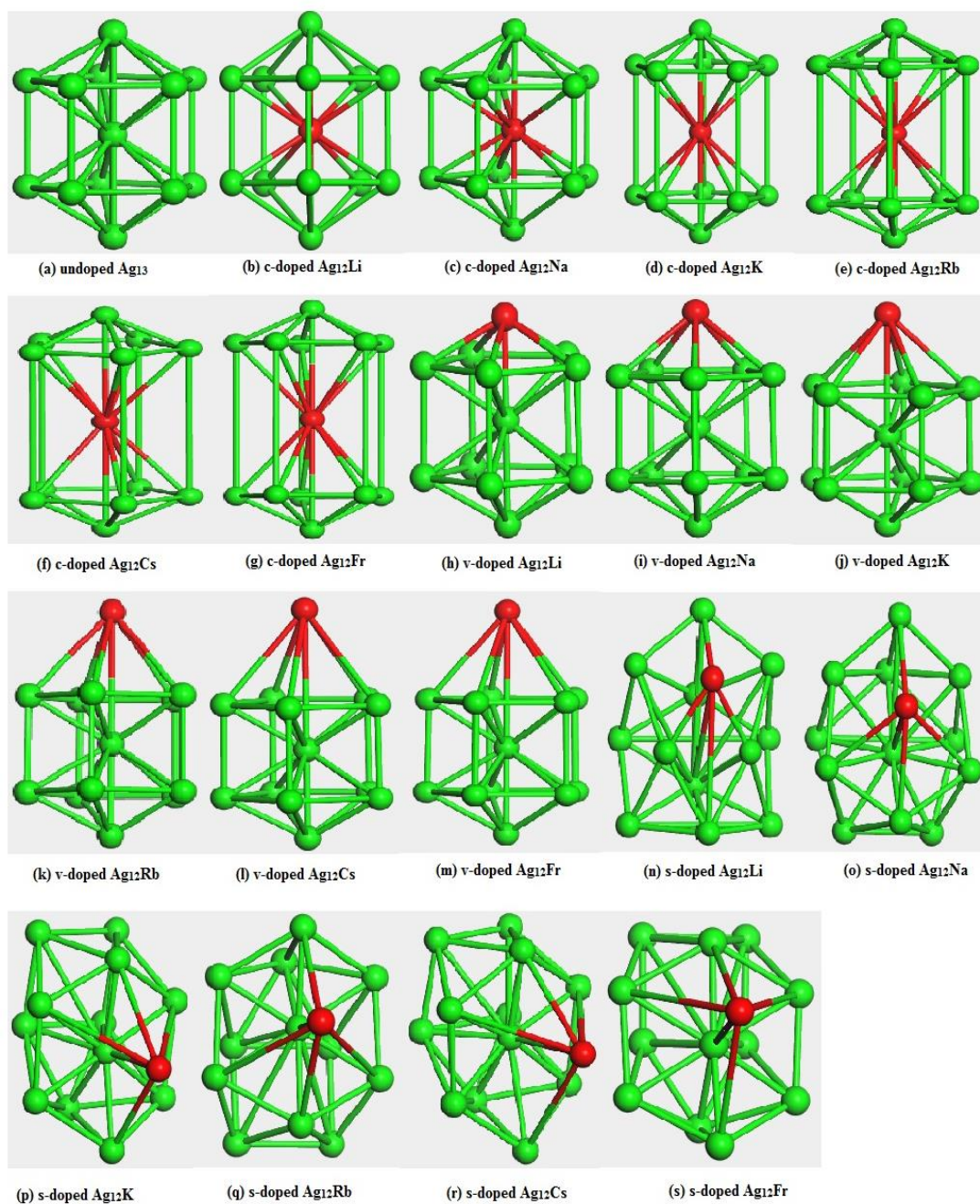


Figure 4.4: Optimized geometry of decahedral Ag_{13} and Ag_{12}X nanoalloys

Table 4.7: Bond length comparison among the undoped and doped clusters

c-doped clusters D_{5h} symmetry	Average bond length A⁰	v-doped clusters C_{5v} symmetry	Average bond length A⁰	s-doped clusters Cs symmetry	Average bond length A⁰
Ag-Ag	2.91	Ag-Ag	2.90	Ag-Ag	2.85
Ag-Li	3.07	Ag-Li	3.49	Ag-Li	2.78
Ag-Na	3.18	Ag-Na	3.27	Ag-Na	3.15
Ag-K	3.29	Ag-K	3.82	Ag-K	3.51
Ag-Rb	3.71	Ag-Rb	3.94	Ag-Rb	3.69
Ag-Cs	4.12	Ag-Cs	4.14	Ag-Cs	3.99
Ag-Fr	4.17	Ag-Fr	4.18	Ag-Fr	4.01

Now, from the data of Table-4.7, it can be clearly seen that Ag₁₂Li and Ag₁₂Na clusters exhibit the minimum geometrical deviation, whereas the maximum deformation is observed from Ag₁₂Cs and Ag₁₂Fr clusters compared to undoped Ag₁₃. Hence, it can be said that the Li and Na doped clusters are supposed to be more stable with respect to Cs and Fr doped clusters. This deforming trend can be easily explained considering the fact that the atomic radii of the doped alkali atoms increases from Li (1.52 A⁰) to Fr (2.82 A⁰), while it maintains an incremental trend (Na: 1.54 A⁰, K: 2.27 A⁰, Rb: 2.48 A⁰, Cs: 2.65 A⁰) down the periodic table group. Besides, all these atomic radii are larger than the atomic radii of Ag (1.44 A⁰). (Emsley) Thus, when doping similar sized atoms (for example Li, Na and) into Ag₁₃ produces the minimum geometrical deviation with respect to the parent Ag₁₃. Similarly, adding larger atoms results with higher geometrical deformation. Now, with the results of structural change as the outcome of doping, it is clearly understood that Li, Na and K doping are more favorable with respect to Rb, Cs and Fr. Moreover, being the bottom there element of group-IA, it is

well known that Rb, Cs and Fr are very reactive elements. Thus, doping with these three elements to reform Ag-alkali metals bimetallic nanoalloy are not practically feasible option. Therefore, in our next section, where will discuss the electronic and optical properties of the Ag-X clusters, our doped elements will be limited to Li, Na and K only, and accordingly $X = \text{Li, Na, K}$.

4.2.2. Electronic properties

After discussing the structural motifs of the doped clusters in the previous section, analysis is then focused on the electronic properties of the clusters and Tables 4.8 and 4.9 have listed the binding energy (BE), vertical ionization potential (VIP), vertical electron affinity (VEA) and HOMO-LUMO gap of the entire c-doped, v-doped and s-doped Ag_{12}X clusters.

Referring to Table 4.8, it can be said through the DFT calculation; the binding energy of decahedral Ag_{13} is predicted to be 19.19 eV, which is similar to the previously reported result from Yi Rao et al (Rao et al., 2013). Referring to the data of Table 4.8 and 4.9, it can clearly be found that amongst all the doped structures only Ag_{12}Li possess higher BE than the corresponding value of Ag_{13} ; hence the Li doped Ag_{12}Li neutral clusters are expected to be more stable than the undoped Ag_{13} clusters. In particular, the s-doped Ag_{12}Li with C_s symmetry exhibits the highest BE amongst all the clusters considered in this paper. It is also observed that the surface or, vertex doped Ag_{12}X clusters displays higher BE compared to c-doped Ag_{12}X compounds, signifying that the favored structure is c-doped Ag_{12}Li and the entire surface doped Ag_{12}X structures. The reason for this observation is as follows: the bulk interatomic distances for Ag, Li, Na, K are 2.89, 3.023, 3.659 and 4.525 Angstroms, respectively. (Kittel, 2005) Thus, the strain for c-doped Ag_{12}X_1 increases in the order $X=\text{Li, Na, K}$ and is larger for the bigger atoms.

Therefore, they prefer the surface doping site. However interestingly, c-doped Ag_{12}Li has higher binding energy than Ag_{13} .

Table 4.8: Binding energy (BE), vertical ionization potential (VIP), vertical electron affinity (VEA) and HOMO-LUMO gaps for Ag_{13} and c-doped Ag_{12}X clusters

Cluster	Symmetry	Spin	BE (eV)	VIP (eV)	VEA (eV)	HOMO-LUMO Gap (eV)
Ag_{13}	D_{5h}	1	19.19	5.61	2.08	0.22
Ag_{12}Li	D_{5h}	1	19.79	5.71	2.20	0.23
Ag_{12}Na	D_{5h}	1	18.71	5.75	2.16	0.19
Ag_{12}K	D_{5h}	1	17.29	5.73	2.79	0.17

Table 4.9: Binding energy (BE), vertical ionization potential (VIP), vertical electron affinity (VEA) and HOMO-LUMO gaps for the v-doped and s-doped Ag_{12}X clusters

Cluster	Symmetry	Spin	BE (eV)	VIP (eV)	VEA (eV)	HOMO-LUMO Gap (eV)
Ag_{12}Li	C_{5v}	1	19.73	5.35	1.76	0.21
	C_5	1	20.06	6.96	1.49	0.20
Ag_{12}Na	C_{5v}	1	19.00	5.35	1.76	0.21
	C_5	1	19.12	5.51	1.78	0.19
Ag_{12}K	C_{5v}	1	18.20	5.32	1.41	0.16
	C_5	1	19.08	5.57	1.32	0.17

On the other hand, the entire c-doped clusters exhibit higher VEA values than Ag_{13} , whereas all the s-doped and v-doped clusters show lower VEA values with respect to Ag_{13} . It suggests that it will take more energy to attach an electron into the c-doped clusters with respect to undoped or surface doped silver clusters. The probable reason behind these higher EA values can be that, when alkali atoms are doped in the center, the Ag atoms in the shell are pulled apart. This phenomenon creates large geometrical change in the cluster, which eventually result into higher values of VEA. On contrary, the low VEA values of the surface doped clusters can be easily explained by comparing the electronegativity between the Ag atoms and the doped atoms. It is a well-known fact that the group IA metals are highly electropositive. Thus, doping a high electropositive atom such as Li, Na or, K in the surface will enable the cluster to possess a higher affinity for electrons compared to the undoped Ag_{13} cluster.

Apart from the BE, VIP and VEA, the energy gap between the HOMO and LUMO is considered as an important quantity for evaluating the electronic stability of clusters. In fact, a cluster with high HOMO-LUMO gap is generally considered as a cluster with high kinetic stability and low chemical reactivity and vice versa. This is due to the fact that energetically it is not favorable to add electrons to a high lying LUMO and to extract electronics from a low lying HOMO, making it difficult to form the activated complex of any potential reaction (Aihara, 1999; Manolopoulos, May, & Down, 1991). From the data of Tables 4.8 and 4.9, it is revealed that GGA functionals predicted a value of 0.22 eV as the HOMO-LUMO gap of Ag_{13} clusters, which confirms the previous report. (Y. Rao et al., 2013) Amongst the doped clusters only c-doped Ag_{12}Li possesses higher HOMO-LUMO gap with respect to Ag_{13} ; hence the aforementioned doped cluster is expected to be more stable and chemically inert than the undoped silver cluster. Also, it has been reported that neutrals clusters with high HOMO-LUMO gaps

are expected to be very active as anions because of their lower values of VEA. (Molina & Hammer, 2005) From the results presented in Table-4.8 and Table-4.9, it is clear that neutral doped clusters (especially Ag_{12}Li) possess high BE and HOMO-LUMO gaps along with low VEA. Therefore, anions of these clusters are expected to be highly reactive compared to the corresponding of undoped Ag_{13} , hence can be good potential candidates for catalysis.

4.2.3. Optical absorption properties

After discussing the structural and electronic properties of the doped clusters, the attention is now towards the key motivation of this thesis, which is the optical spectrum of the doped clusters. Figure 4.5a shows the optical spectra of Ag_{13} , where it is clearly seen that the silver cluster has its optical spectrum range in between 330 to 400 nm while its peak is found at 360 nm (3.44 eV) wavelength, which is an excellent match to the previously reported experimental spectra of Ag_{13} (Weissker & Mottet, 2011; Ma & Chen, 2012). Kitaev et al. (Pietrobon & Kitaev, 2008) has reported the experimental optical absorption spectra of the 35-123 nm sized decahedral silver nanoparticles in the range of 455-570 nm wavelength. However, it is well known that the optical peaks of the nanoparticles are red-shifted with the increment of the particle size. (Harb et al., 2008; Cai et al., 2009) Thus absorption spectra of our investigated 13-atom silver cluster, which is significantly smaller with respect to those 35-123 nm sized particles, is consistent with the anticipation of a blue shift for smaller particles.

Referring to the optical spectra of the doped clusters of Figure 4.5b, 4.5c and 4.5d, the effect of doping in the optical properties can be described as follows. All the c-doped Ag_{12}X clusters optical peak are red-shifted with respect to undoped Ag_{13} , whilst c-doped Ag_{12}Na exhibits excellent optical oscillation strength with its peak in the range of

370-390 nm wavelength. On the other hand, the entire v-doped clusters display wider absorption spectra ranged 300-600 nm compared to the parent Ag₁₃. Moreover, the optical peak of v-doped Ag₁₂Li and Ag₁₂Na dimers are slightly blue-shifted, whereas a red-shifted peak was observed from Ag₁₂K with respect to parent Ag₁₃. The third group of doped clusters i.e. the s-doped clusters exhibit very interesting optical spectra. Amongst these clusters, the optical peak of Na-doped clusters is red-shifted, whilst the Li and K doped clusters show their optical peak exactly in the same wavelength of silver. But interestingly, the Li doped cluster exhibit remarkable absorption strength, which is almost 3 times higher than the undoped Ag₁₃ dimer. On the contrary, it is reported that the increment of cluster size in a pure metallic nanoparticle system results to red-shift in optical bands, whereas blue-shift occurs as result of decrement of cluster size. (M. Harb et al., 2008) (Cai et al., 2009) Thus, it links up the relation between the optical spectra and the geometrical structures of the bimetallic clusters.

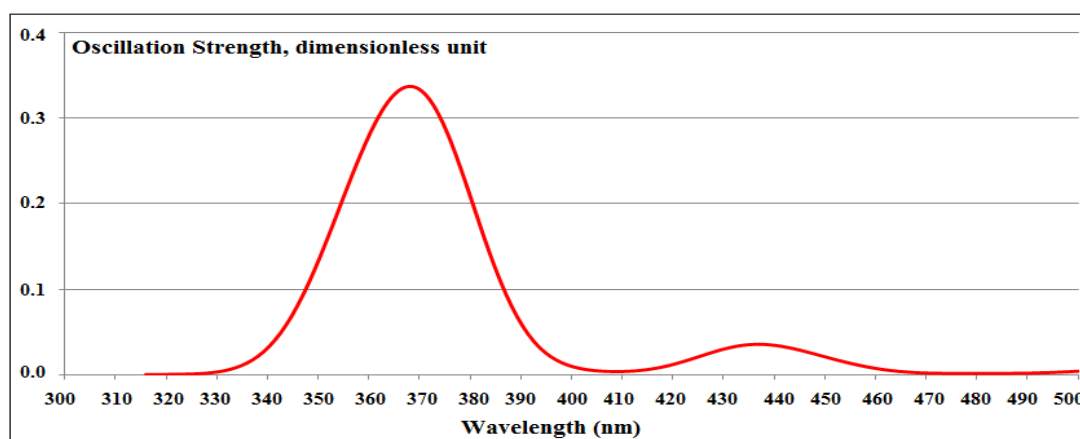


Figure 4.5(a): Optical absorption spectra of decahedral Ag₁₃

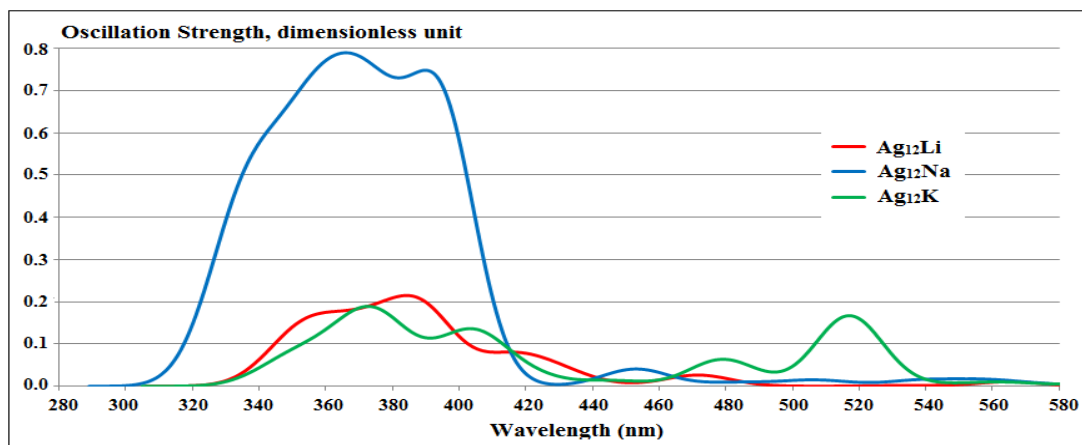


Figure 4.5(b): Optical absorption spectra of c-doped Ag_{12}X clusters

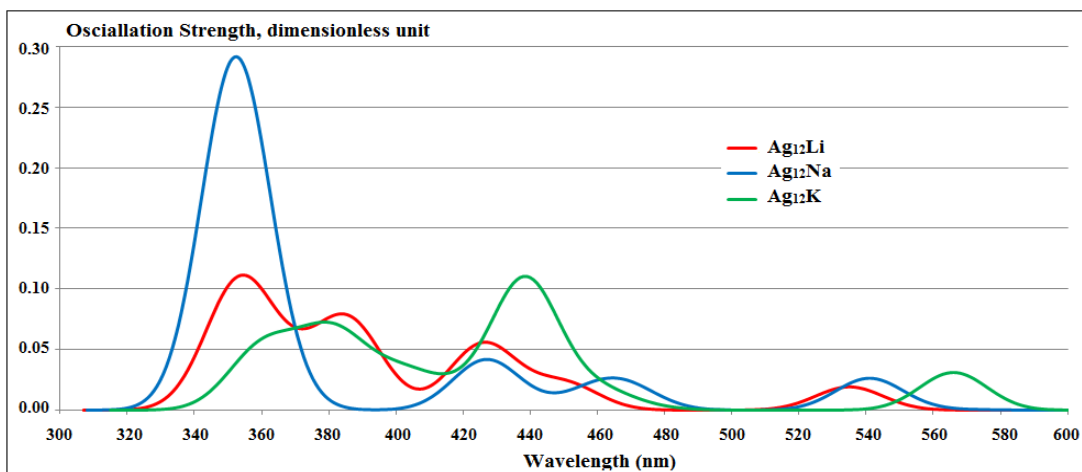


Figure 4.5(c): Optical absorption spectra of v-doped Ag_{12}X clusters

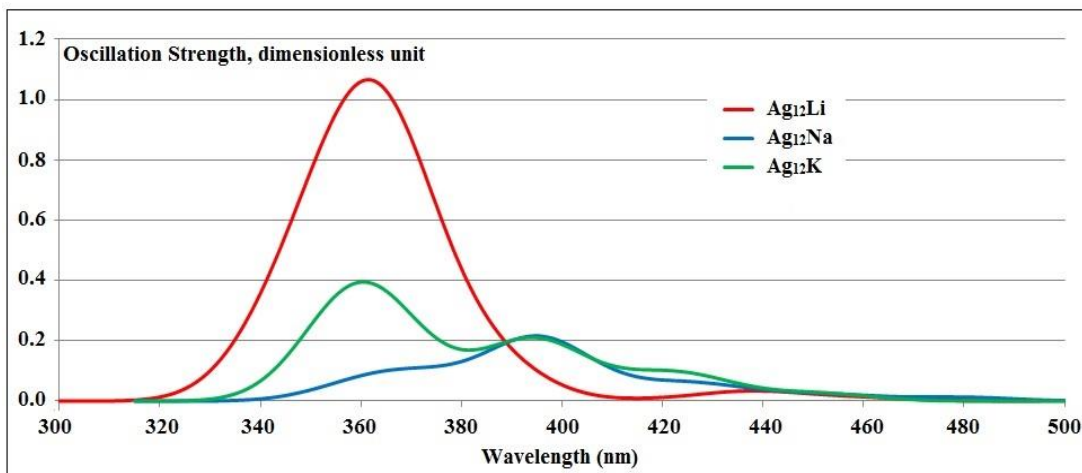


Figure 4.5(d): Optical absorption spectra of s-doped Ag_{12}X clusters

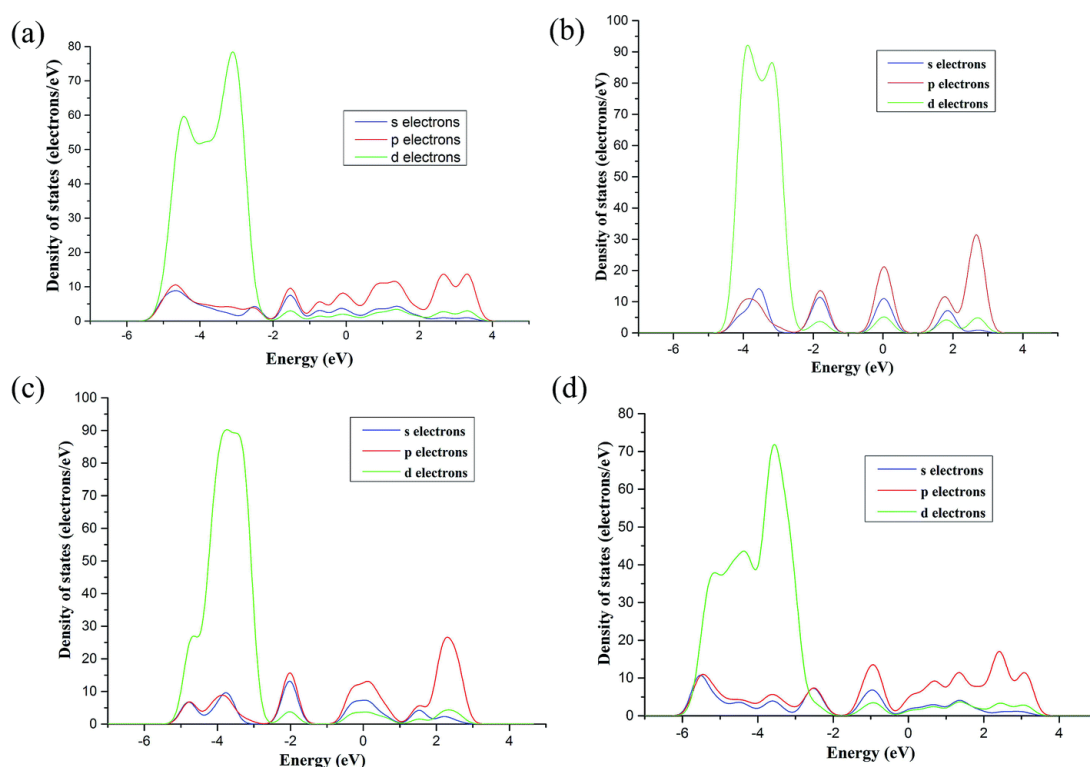


Figure 4.6: PDOS of (a) decahedral Ag_{13} , (b) c-doped Ag_{12}Li , (c) v-doped Ag_{12}Li , (d) s-doped Ag_{12}Li clusters

With reference to the optical spectra of the doped clusters, let's move our focus towards the electronic evolution of the spectra of the doped clusters. Here, with the presence of alkali atoms these bimetallic Ag_{12}X clusters in the excited states lead to a quasi-continuum spectrum. In particular, for the case of Ag_{13} , the electronic transitions are happening as a result of excitations from the s and d orbitals. These s and d orbitals are well localized in surface silver atoms, along with its evolution as hybrid s-p orbitals in the wide areas of outer region where several atoms are involved with the system. (Harb et al., 2010) On the contrary, the absorption spectra of alkali metal clusters are explained as collective oscillation of *s valence electrons* and the shift of absorption energies of very small particles, compared to the larger ones explained by a spill out (extension of the electronic wave functions out of the “classical volume” of the cluster)

of these *s-electrons*. (Harb et al., 2008) Thus, when alkali metal is doped into the noble metal cluster, a systematic investigation of the excitations in molecular level is quite complicated. Investigation of the absorption spectrum of the clusters through the partial density of states (PDOS) calculation is shown in Figure 4.6 by the PDOS of Ag_{13} , c-doped, s-doped and v-doped Ag_{12}Li . From the PDOS of Figure 4.6 (a-d), it is clearly observed that the actions of d orbitals in Ag_{13} are more dominant in the energy range of -2 to -5.5 eV, with its peak at -3.15 eV. For the cases of c-doped, v-doped and s-doped Ag_{12}Li , we find that the d electrons still exhibit the stronger role, but their peaks are red-shifted to -3.9 eV, -3.75 eV and -3.55 eV respectively, which indicates that d electrons are transferred to higher energy level for the doped clusters. In actual fact the doping of Li into the Ag nanoparticles results an increase in the occupation of empty s and p bands of the Ag_{13} cluster, which eventually causes the d electrons transferred to higher energy level. Thus, this transfer of d electrons potentially well-explain the red-shifting or, blue-shifting of optical spectra of the doped Ag_{12}X clusters.

Overall, it can be concluded that the c-doped and v-doped Ag_{12}Na and s-doped Ag_{12}Li are the most favorable clusters if the higher oscillation strength is the criteria, whereas the entire c-doped and v-doped clusters exhibit wider ranged absorption spectra with respect to undoped Ag_{13} .

4.3. Structural stability and the electronic, chemical and optical properties of 13-atoms icosahedral Al_{12}X and Cu_{12}X structures

In order to check the ground state structures as well as electronic and optical properties of the alkali atoms doped Al_{12}X and Cu_{12}X clusters, one Al and Cu atom is substituted in core and surface positions of a 13 atoms icosahedral Al_{13} and Cu_{13} structures by an alkali atoms (here we have considered Li and Na only, hence $\text{X}=\text{Li, Na}$) to form c-

doped and s-doped Al_{12}X and Cu_{12}X bimetallic clusters respectively. The entire c-doped and s-doped Al_{12}X and Cu_{12}X neutral and charged clusters were geometrically optimized without imposing symmetry by nonlocal functional Generalized Gradient Approximation (GGA) with PBE as exchange functions and DNP as basis set. The ground state of all clusters was determined by checking their total energy and binding energy with different spin multiplicity from singlet to octet to find the most stable structures.

4.3.1. Geometry optimization and energetic stability

Figure-4.7 shows the geometrically optimized structures of all the Al_{12}X and Cu_{12}X clusters, as well as their optimized symmetry and best-fit spin multiplicity. From the figure, it is evident that Cu_{13} has maintained the I_h symmetry with sextet spin multiplicity, whereas Al_{13} gets optimized to a slightly distorted icosahedron of D_{3d} symmetry with doublet spin multiplicity, which confirms the previous study as well. (Ma & Chen, 2012; B. K. Rao & Jena, 1999) Among the doped clusters core-doping didn't affect the home-symmetry as the core-doped clusters maintained the same icosahedron symmetry, whereas surface doping has resulted change in symmetry, which are depicted in the figure. Now, harmonic vibrational frequencies calculations have been carried away in order check the stability of the entire pure and doped clusters, where stability of the clusters are confirmed by the absence of imaginary frequencies. The lowest and highest vibrational frequencies of the clusters are charted in Table-4.10. In our calculation, we haven't witnessed any imaginary vibrational frequency for any of the optimized clusters of Figure-4.7; hence all the pure and doped clusters are geometrically stable.

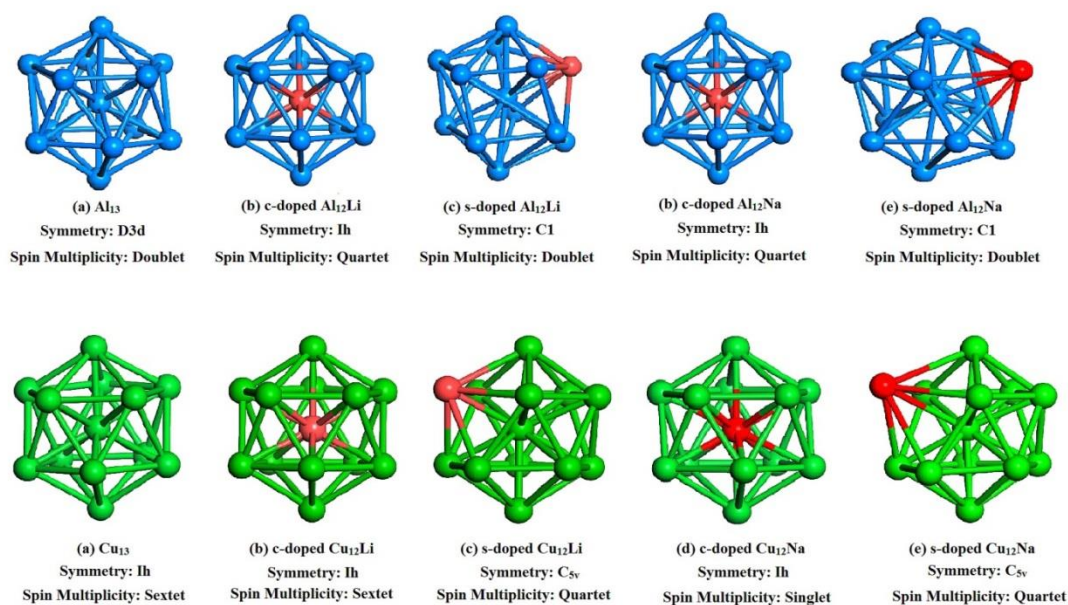


Figure 4.7: Optimized geometry of Al_{12}X and Cu_{12}X clusters

Table 4.10: Lowest and highest vibrational frequency of the Al_{12}X and Cu_{12}X clusters

Compound	Lowest Vibrational Frequency cm^{-1}	Highest Vibrational Frequency cm^{-1}	Compound	Lowest Vibrational Frequency cm^{-1}	Highest Vibrational Frequency cm^{-1}
Al_{13}	10.48	372.84	Cu_{13}	61.22	282.71
c-doped Al_{12}Li	69.32	477.80	c-doped Cu_{12}Li	88.36	586.75
s-doped Al_{12}Li	29.54	381.43	s-doped Cu_{12}Li	40.20	365.44
c-doped Al_{12}Na	24.41	392.96	c-doped Cu_{12}Na	62.69	392.62
s-doped Al_{12}Na	17.98	364.70	s-doped Cu_{12}Na	44.35	273.5

4.3.2. Electronic properties

Tables 4.11 and 4.12 are compiled with the binding energy (BE), vertical ionization potential (VIP), vertical electron affinity (VEA) and HOMO-LUMO gap for all the doped clusters. It is apparent that Al_{13} and Cu_{13} have binding energy of 33.44 eV and

28.51 eV and regarding the VIP value, they exhibit values of 6.82 eV and 6.07 eV respectively, which confirms the previous reports and verify the suitability of our selected computational functional and basis sets as well. (Candido, Rabelo, Da Silva, & Hai, 2012; Kumar, 1998; Ma & Chen, 2012; Neogrady, Kellö, Urban, & Sadlej, 1998; Ouyang, Wang, Xiang, Chen, & Du, 2012; Y. Rao et al., 2013) Now among all the bimetallic clusters, the s-doped Al-X and Cu-X clusters exhibit slightly higher binding energies than their core doped counterparts. This is because the atomic size of both of Li and Na are larger than Al and Cu. Thus, caging the X atom in the center of core-shell structures surrounded by Al and Cu atoms offer lesser stability than placing the X atoms in the surface; signifying that the surface doping is the preferred position with little higher electronic stability.

Table-4.11: Binding Energy (BE), Vertical Ionization Potential (VIP), Vertical Electron Affinity (VEA) and HOMO-LUMO gap of the Cu_{13} and the Cu_{12}X clusters. All data are in eV.

Compound	BE	VIP	VEA	HOMO-LUMO Gap
Al_{13}	33.44	6.82	3.01	1.16
c-doped Al_{12}Li	30.89	6.59	2.82	1.29
s-doped Al_{12}Li	32.23	6.25	1.84	1.08
c-doped Al_{12}Na	27.94	6.09	2.47	1.22
s-doped Al_{12}Na	31.68	6.03	2.39	1.06

Table-4.12: Binding Energy (BE), Vertical Ionization Potential (VIP), Vertical Electron Affinity (VEA) and HOMO-LUMO gap of the Al₁₃ and the Al₁₂X clusters. All data are in eV.

Compound	BE	VIP	VEA	HOMO-LUMO Gap
Cu ₁₃	28.51	6.07	2.02	1.34
c-doped Cu ₁₂ Li	27.77	6.23	2.12	1.32
s-doped Cu ₁₂ Li	28.00	5.71	1.94	1.05
c-doped Cu ₁₂ Na	24.65	6.21	2.08	1.28
s-doped Cu ₁₂ Na	27.43	5.58	1.82	1.02

The higher value of IP specifies a deeper HOMO energy level, signifying that the structures with large value of IP are expected to be chemically more stable or, exhibiting lesser chemical reactivity. On the contrary, higher value of EA indicates a more solid binding between the cluster and an electron. From the calculations tabled here, it is obvious that the IP values are higher for the core-doped clusters compared to their s-doped counterparts. Moreover, Cu₁₂Li cluster possesses higher IP with respect to Cu₁₃; hence this center doped alloyed cluster is expected to be chemically more stable compared to its pure counterpart. On the other hand, similar behavior is also observed regarding the doped clusters electron affinity, where the core doped clusters retain more EA compared to their surface doped counterparts. Furthermore, both of Li and Na core doping into Cu has resulted higher electron affinity with regard to Cu₁₃ clusters. Now, when highly electropositive atoms like Li and Na is doped into the Al and Cu cluster, the large difference between the Pauling electronegativity between the home cluster and the doped cluster results some ionic bonding as well. Again, this ionic bonding becomes

more acute when the doped atom is placed into the core of a core-shell structure rather than in the surface. This is because core-doping enables the doped atom to sit in the center and get into bond-involvement with more home atoms compared to the shell doped atom. Thus, it explains the higher IP and EA; hence greater chemical stability of the core-doped $Al_{12}X$ and $Cu_{12}X$ clusters.

The energy gap between the HOMO and LUMO is considered as an important quantity for evaluating the electronic stability of clusters. In fact, it is well known that the magic-clusters with high symmetry and closer electronic shells have large HOMO-LUMO gaps; hence the clusters are generally stable and unreactive. (Yildirim et al., 2011) But despite of the immense utility of the MO theory, commonly used DFT functional are seen not predicting the orbital energies accurately. (G. Zhang & Musgrave, 2007) On the other hand, Koopmans's theory recommends that at the Hatree-Fock (HF) level the eigen value of HOMO energy should be a good approximation to predict the negative experimental IP. (Cramer, 2013) Similarly, the LUMO energy should be equal to the negative value of EA considering the assumption that the orbitals do not relax. But the reliability of the Koopmans's theory for predicting EA is question worthy due to its significant effect of orbital relaxation over the Eigen value of LUMO energy. (Garza et al., 2000) Therefore, the accuracy of a functional method is generally tested by comparing the HOMO energy and negative IP of the clusters. Zhan et al (Zhan et al., 2003) examined the HOMO eigenvalues along with HOMO-LUMO gap of some clusters with B3LYP functional and found there exists linear correlation between the B3LYP predicted values with the corresponding experimental values. Thus, based on the above mentioned reports, we have used B3LYP functional for calculating the HOMO-LUMO gaps of all the clusters considered in this paper.

From the data presented in Table-4.11 and Table-4.12, it is evident that all the clusters presented here possess high values for HOMO-LUMO gaps. More specifically, Li and Na doping into the core of Al clusters have given rise to the increment of HOMO-LUMO gaps with respect to its pure copper clusters. It implies that, both of the core-doped clusters are chemically and electronically more stable compared to their undoped counterpart. Similar behavior is seen in the doped Cu clusters as well, while c-doped Cu_{12}X clusters exhibit higher HOMO-LUMO gaps. Expectedly, in both cases, core doping has resulted higher HOMO-LUMO gaps, i.e. higher electronic stability compared to surface doping as explained in the previous part.

After the discussion of the electronic attributes of the Al_{12}X and Cu_{12}X clusters it is evident that the doped clusters retain excellent electronic and chemical stability. The neutrals clusters with high HOMO-LUMO gaps are expected to be very active as anions due to their lower values of VEA. (Molina & Hammer, 2005) Here the Al_{12}X and Cu_{12}X clusters, exhibit high HOMO-LUMO energy gap with low electron affinity. Thus, the doped clusters especially the core-doped clusters can be excellent potential for catalytic applications.

4.3.3. Optical absorption properties

Absorption spectra of doped clusters are showed in Figures 4.8-4.10. They give the oscillator strength as a function of the excitation energy, together with a curve obtained by a Lorentzian broadening (with a full width at half-maximum of 0.1 eV). Spectra include calculated excitation energies up to 6 eV and 11 eV for Cu clusters and Al clusters respectively. The spectrum of Cu_{13} is characterized by an intense and narrow band centered at 3.55 eV, and some much less intense transitions above 5 eV. Substituting a Cu atom by an alkali atom, either in surface or in the core, leads to a

broadening of the band main band. The doping in surface with Li and Na leads to an increase of the optical response in the entire energy domain above 2.2 eV, with new peaks well scattering on all the range of energy. It is particularly strong in the UV but also in the visible domain. The optical response increases also when the substitution is made in the core. In that case, the increase is stronger in the UV domain than in the visible one.

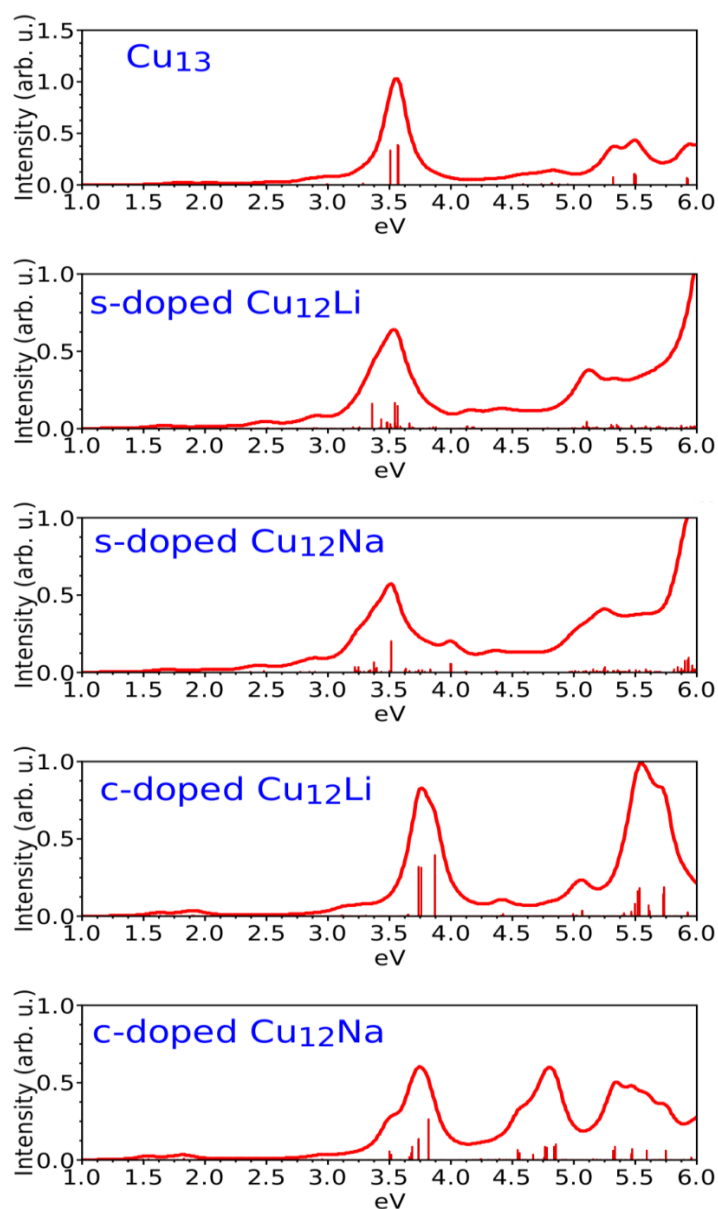


Figure-4.8: Absorption spectra of Cu_{13} and Cu_{12}X ($\text{X}=\text{Li}, \text{Na}$) clusters.

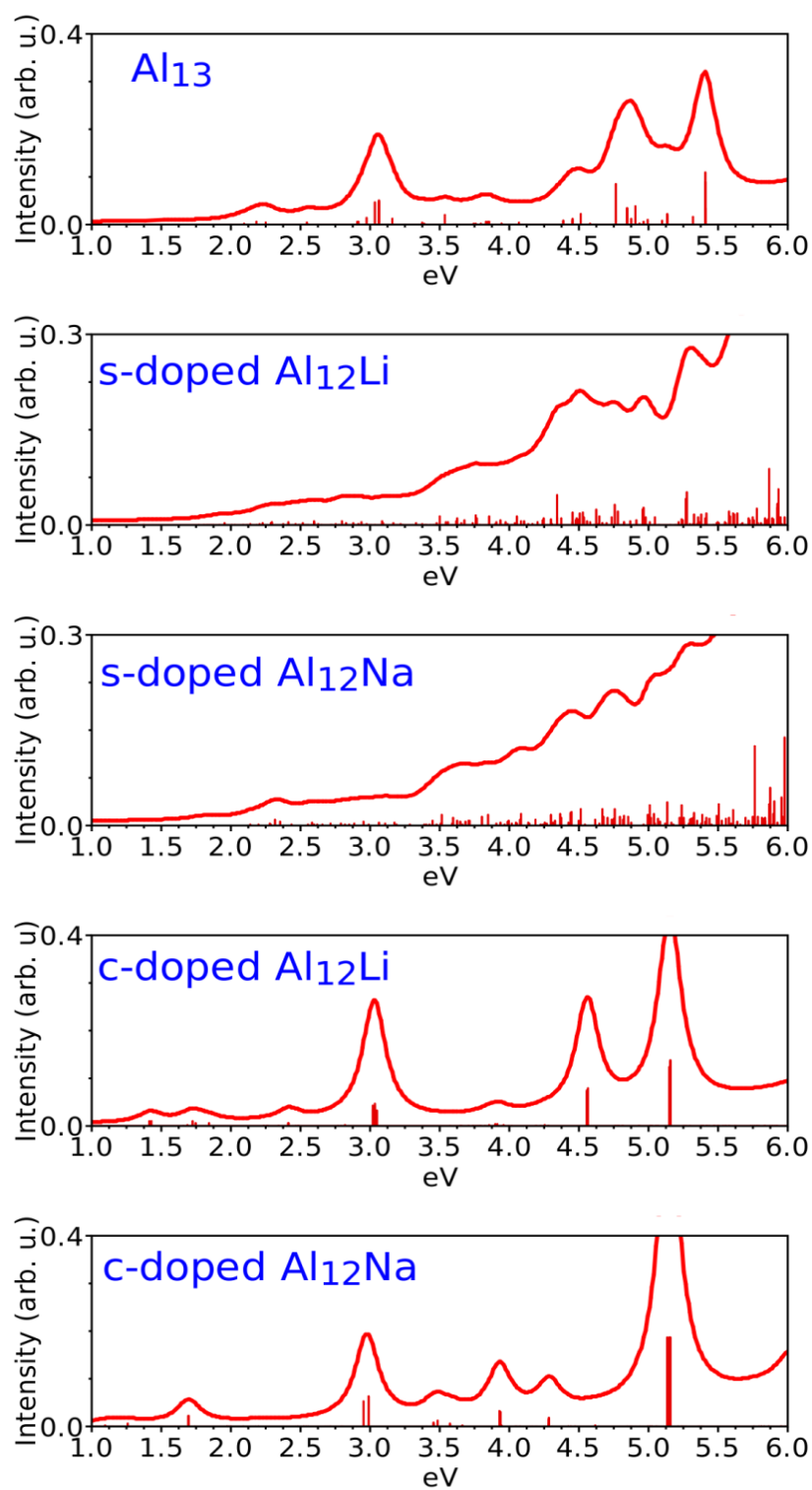


Figure-4.9: Absorption spectra of Al₁₃ and Al₁₂X (X=Li, Na) clusters up to 6 eV

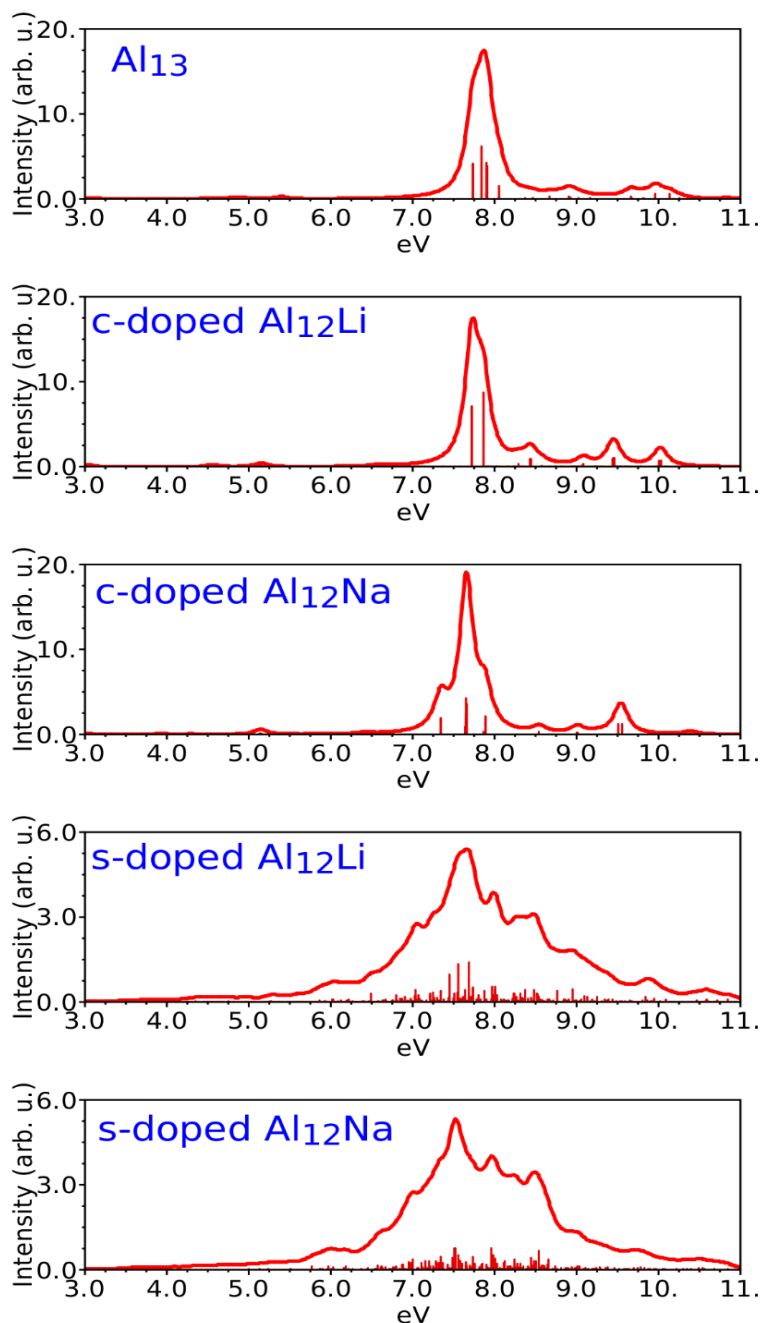


Figure-4.10: Absorption spectra of Al_{13} and $Al_{12}X$ ($X=Li, Na$) clusters up to 11 eV

For aluminum, the optical response is lower in the 1-6 eV range (Figure 4.9) of excitation energy than for copper. The spectrum of undoped Al_{13} show some relatively intense peaks at about 3.0, 4.7 5.4 eV. The doping with Li or Na atom in surface lead to significant changes with the emergence of a very large band composed of many excited

states well dispersed in the entire energy domain. The density of excited states becomes stronger in the UV. In contrast, spectra of c-doped clusters show very few peaks and are somewhat similar to that of undoped Al_{13} , because the high Ih symmetry is preserved.

Figure 4.10 shows the optical spectra of Al_{13} and Al_{12}X clusters up to 11 eV, where Al_{13} exhibits its optical peak in 7.75, 7.85 and 7.89 eV. For the core-doping, the doped clusters show similar optical behavior with respect to undoped aluminum. In contrary, surface doping has yielded significant improvements, where a large absorption band gap is observed for the s-doped Al_{12}X clusters, comprises from 4 to 11 eV in UV range.

It is revealed that the doping of Li and Na has made the absorption bandgap wider with regards to undoped Al_{13} and Cu_{13} in the UV and UV-Vis regions. Typically optoelectronic devices such as solar cells absorb lights in the range of 1-6 eV. The calculation proved that Li and Na doping has improved the absorption bandwidth in the mentioned range. Hence the wider bandgap will allow increasing the photo current as well as the optical absorption efficiency.

On the contrary, the most widely used nanomaterials for solar cells are gold and silver that have their absorption peaks in the visible optic range and thus correspond more powerfully with the peak solar intensity (Fahim et al., 2012; Pillai et al., 2007; Y. Zhang et al., 2012). However, at the short wavelengths such noble metals are found less effective in absorbing light because of the destructive interference between the scattered and unscattered light below their corresponding resonance point and hence, the solar cell efficiency falls down, which is well-explained by the Fano-effect (Kroner et al., 2008; Z.-J. Yang et al., 2011; Y. Zhang et al., 2012). Here, the peak optical absorption of both of the Al_{12}X and Cu_{12}X clusters fall into UV and UV-Vis region, which implies that these doped clusters will not produce the negative affect in the solar cells as like as

Ag and Au, arisen by the destructive interference i.e. Fano-effect. In addition, doping of Li and Na into surface of Al has made the $Al_{12}X$ clusters to absorb light in a very wide range of 4eV to 11 eV. Such wide bandgap UV light absorber is rare and hence, $Al_{12}X$ clusters can be an excellent material for UV-absorber or, UV-emitter. Thus, these Li and Na doped Al clusters may find its potential applications in UV light therapy (Elman & Lebzelter, 2004; Hearn et al., 2008) and several UV absorbing applications (Becheri et al., 2008; Koutchma et al., 2009) as well.

4.4. Summary

In this chapter the geometrical stability and the electronic, chemical and optical properties of the icosahedral $Ag_{12}X$, $Cu_{12}X$ and $Al_{12}X$ have been discussed comprehensively. The electronic and optical properties of all doped and undoped clusters have been calculated in the framework of density functional theory (DFT and TDDFT). To investigate the doped cluster, we have replaced one Ag, Al and Cu atom from the core (c-doped) and surface (s-doped) of a 13 atom icosahedral structure by an alkali atom (X) to form c-doped and s-doped $Ag_{12}X$, $Al_{12}X$ and $Cu_{12}X$ clusters respectively. For the decahedral Ag-X alloys, we have added one more doping position in the vertex, which is regarded as v-doped $Ag_{12}X$ clusters. Later, the structural stability of the doped clusters was ensured by vibrational analysis and bond length comparison. To analyze the electronic and chemical stability of the doped clusters, the calculations of BE, VIP, VEA and HOMO-LUMO gaps were performed. Finally the optical properties of the clusters were calculated in the framework of TDDFT with ALDA-kernal as the exchange correlation function which was followed by partial density of states (PDOS) calculation to correlate between the electronic evolution and optical absorption spectra.

Amongst the Ag_{12}X clusters, Li, Na and K doped clusters resulted least distortion from undoped Ag_{13} cluster; hence imply the best stability. It is observed that the Ag_{12}Li clusters have higher BE than the parent Ag_{13} cluster; hence Li doped cluster is the more favored amongst all the doped clusters considered. All the doped clusters have exhibited high values of VIP; hence the doped clusters are expected not to lose electrons easily. Moreover, we observe higher VEA values for the c-doped clusters compared to Ag_{13} and the surface doped clusters; implying that the s-doped clusters hang around with electrons more easily with respect to c-doped Ag_{12}X clusters. Regarding the HOMO-LUMO gap, all the doped clusters showed high values; hence anions of the doped clusters are expected to be very reactive. Thus, these Ag_{12}X clusters, specially the Ag_{12}Li and Ag_{12}K can be excellent potential for catalytic applications. Regarding the optical properties, all the Ag_{12}X clusters have exhibited excellent optical properties, when the doping has resulted red-shifting in the optical peaks with respect to undoped ones. Importantly, all the doped clusters have shown increased optical intensity in the visible optical range. Thus these Ag-X nanoalloys can be an excellent potential for optoelectronic applications, especially for thin film solar cells.

Next, when we moved our focus towards Al-X and Cu-X alloys, the high values of binding energy and vertical ionization potential have ensured the electronic stability and chemical inertness of the doped clusters. Furthermore, large energy gap between the HOMO and LUMO along with low electron affinity of the Al_{12}X and Cu_{12}X clusters is observed, which has made us believe that these doped clusters can be an excellent and low cost alternative to silver and gold nanoparticles for the catalytic applications. In the optical part, alkali atoms doping into Cu have significantly improved the optical intensity in the UV-Vis regions; hence these clusters can be an excellent low cost alternative for Ag or, Au in plasmonic solar cells. On the other hand, Al generally

absorbs light in the UV regions, whereas for solar cells, lights more than 5eV energy do not come to much of the use. Thus, Al-X alloys might not be very useful for solar cells. But interestingly $Al_{12}X$ have exhibited large absorption bandgap in the UV absorption. Therefore, Al-X alloys can be an excellent potential for UV absorption applications such as UV-therapy and several UV protectors.

Thus, it can be concluded saying that all the Ag-X, Al-X and Cu-X possess interesting properties which can find its applications in opto-electronics, catalysis. In addition, Al-X can be an excellent potential for UV-absorption applications.

CHAPTER 5

CONCLUSION

As we go forward, I hope we're going to continue to use technology to make really big differences in how people live and work.

Sergey Brin, the co-founder of Google said this. Since the first concept of nanotechnology came through the hand of Richard Feynman in 1959, it has turned to the mostly researched topic in today's world and here we have presented our slightest contribution towards the vast sea of nanotechnology research.

The major motivation of this research work was to find alternative plasmonic materials of silver and gold, which is cheaper, chemically more stable and exhibit better optical properties. Among the options available, alkali metals are reported as the best plasmonic materials, whereas copper and aluminum possess attractive properties and more importantly, they are cheaper. But unfortunately alkali metals are very reactive to air and water and none of Cu and Al exhibit plasmonic quality as good as silver or gold. With an aim to solve this problem, we came with an idea of doping alkali metals into the silver, copper and aluminum to find whether doping results significant improvement in the aforementioned nanoalloys.

For this work, we have selected 13-atoms core-shell structures as the quantum model of Ag-X, Al-X and Cu-X nanoalloys. Later, DFT calculations have been carried out to evaluate the geometrical and energetic stability of the nanoalloys. In addition, binding energy (BE), vertical ionization potential (VIP), vertical electron affinity (VEA) and HOMO-LUMO gaps were determined to compare the electronic stability and chemical

inertness of the doped clusters. Finally, TDDFT calculations were carried out to compute the optical absorption spectra of the nanoalloys

All of the Li and Na doped clusters have exhibited high chemical stability, whereas their anions are found very reactive. Thus, all of the aforesaid Li and Na doped clusters can be excellent potential for catalytic applications. In addition, doping has yielded significant changes in the optical absorption spectra of the nanoalloys, with respect to their undoped counterparts. For the Ag-X and Cu-X nanoalloys, noticeable improvement was observed in absorption intensity in visible and UV-Vis optical ranges as a result of doping. Typically, solar cells absorb light in the visible and UV-Vis regions, hence these Ag-X and Cu-X clusters can bring attention-grabbing heightening as a replacement of silver and gold nanoparticles in the thin film solar cells, as well as other opto-electronic applications. On the contrary, Al-X clusters are found to exhibit remarkable wide optical absorption band gap in UV optical spectra, for why it would be an excellent potential for UV-absorption applications such as UV-therapy, UV-coating and etc.

In light of the discussions above, it can be concluded that these Ag-X, Al-X and Cu-X nanoalloys have attractive chemical and optical properties, which can make them as excellent potential as the alternative plasmonic materials of silver and gold. Here, Ag-X is an improvement over Ag, whereas both of the Al-X and Cu-X nanoalloys are the cheaper alternatives of silver and gold.

For the future work, we will aim to sort out the limitations of these systems. We propose the followings:

- 1) Fabricating these nanoalloys in a cost effective way is a challenging work. To date there is only one report on Ag-Li fabrication (Lee et al., 2010). For Al-Li alloys, they have been in use for long years as airplane material but mostly as bulk materials. So, in our future work we will focus on finding a cost effective way to fabricate these alloys in nano-scale with controlled size and shape.
- 2) In our materials, we have used 12:1 ratio for the doping. In future, several other ratios will be tested to find whether it brings any improvement over the previous ones.
- 3) We all know about the metal's reactive nature towards air and water. As we have used metal alloys here, we are planning to add a polymer compound over the metallic alloys to keep the metals free from the touch of air and water. The polymer needs to be optically opaque for the needed optical frequency range and has to be conductive.

In this work we have tried to find out an alternative plasmonic material of the expensive silver and gold. Finally it can be concluded that these Ag-X, Al-X and Cu-X nanoalloys possess attention-grabbing chemical and optical properties, which can come as low cost alternative of silver and gold nanoparticles. In addition, there is room of improvement as well by using the above-mentioned future work plans.

Most probably, the introduction of formal science came through the hand of the Greek philosopher and scientist Thales of Miletus in the years around 600 BC. In this long period of time hundreds and thousands of scientists have come and leaded the world

towards civilization. In that vast sea of knowledge, here, I am putting my nano-contribution in the search of low cost plasmonic material just to play my part, just to accomplish what Richard Feynman said, “*Our responsibility is to do what we can, learn what we can, improve the solutions, and pass them on.*”

APPENDIX A

PUBLICATIONS AND CONFERENCE

Publication

1. **Shaikat Debnath**, Suhana Mohd Said, Muhammad Faris Roslan, Mohd Faizul Mohd Sabri, Bui Duc Long. “A DFT study on alkali atoms doped decahedral silver nanocluster for the potential application in opto-electronics and catalysis.” **RSC Advances**, 5(10), 7665-7672, 2015. (Q1, Impact factor: 3.706)
2. **Shaikat Debnath**, Suhana Mohd Said, Franck Rabilloud, Mohammad Mamunur Rashid, Azizah Mainal. “Cu-X and Al-X [X=Li, Na] nano-alloys as low cost alternative to silver and gold for plasmonic applications” **RSC Advances**, 5(72), 58128-58135. (Q1, Impact factor: 3.706)

Conference

Shaikat Debnath, Suhana Mohd Said. “Structural and Electronic Properties of Li doped Decahedral $Ag_{12}Li$ Bimetallic Nanoclusters”. IEEE International Conference on Semiconductor Electronics (ICSE), Kuala Lumpur, Malaysia, 27-29 August, 2014.

Publications under review

1. **Shaikat Debnath**, Suhana Mohd Said, Abhijit Chatterjee, Franck Rabilloud, Muhammad Faris Roslan, Azizah Mainal “A DFT study on electronic and optical properties of Icosahedral $Ag_{12}X$ [X=Li, Na, K, Rb, Cs, Fr] bimetallic nanocluster for potential applications in opto-electronics and catalysis.”
2. **Shaikat Debnath**, Suhana Mohd Said, Franck Rabilloud, Azizah Mainal, Mohamad Syafie Mahmood. “A DFT study on chemical and optical properties of 7-atoms Ag_mX_{7-m} [X=Li, Na] nanoalloys for potential applications in opto-electronics and catalysis”

REFERENCES

- Aihara, J.-i. (1999). Reduced HOMO–LUMO Gap as an Index of Kinetic Stability for Polycyclic Aromatic Hydrocarbons. *The Journal of Physical Chemistry A*, 103(37), 7487-7495.
- Alamanova, D., Grigoryan, V. G., & Springborg, M. (2007). Theoretical study of the structure and energetics of silver clusters. *The Journal of Physical Chemistry C*, 111(34), 12577-12587.
- Arnold, M. D., & Blaber, M. G. (2009). Optical performance and metallic absorption in nanoplasmonic systems. *Optics express*, 17(5), 3835-3847.
- Ashman, C., Khanna, S., & Pederson, M. (2002). Electron attachment and dynamics of alkali atoms in Al₁₃X (X= Li–Cs) clusters. *Physical Review B*, 66(19), 193408.
- Baldelli, S., Eppler, A. S., Anderson, E., Shen, Y.-R., & Somorjai, G. A. (2000). Surface enhanced sum frequency generation of carbon monoxide adsorbed on platinum nanoparticle arrays. *The Journal of Chemical Physics*, 113(13), 5432-5438.
- Barnard, N. C., Brown, S. G. R., Devred, F., Bakker, J. W., Nieuwenhuys, B. E., & Adkins, N. J. (2011). A quantitative investigation of the structure of Raney-Ni catalyst material using both computer simulation and experimental measurements. *Journal of Catalysis*, 281(2), 300-308.
- Becheri, A., Dürr, M., Nostro, P. L., & Baglioni, P. (2008). Synthesis and characterization of zinc oxide nanoparticles: application to textiles as UV-absorbers. *Journal of Nanoparticle Research*, 10(4), 679-689.
- Berry, R. S., & Haberland, H. (1994). Introduction. In H. Haberland (Ed.), *Clusters of Atoms and Molecules* (Vol. 52, pp. 1-12): Springer Berlin Heidelberg.
- Blaber, M. G., Arnold, M. D., & Ford, M. J. (2009a). Designing materials for plasmonic systems. *arXiv preprint arXiv:0908.3707*.

- Blaber, M. G., Arnold, M. D., & Ford, M. J. (2009b). Search for the ideal plasmonic nanoshell: the effects of surface scattering and alternatives to gold and silver. *The Journal of Physical Chemistry C*, 113(8), 3041-3045.
- Blaber, M. G., Arnold, M. D., & Ford, M. J. (2010). A review of the optical properties of alloys and intermetallics for plasmonics. *Journal of Physics: Condensed Matter*, 22(14), 143201.
- Bouillard, J.-S. G., Dickson, W., O'Connor, D. P., Wurtz, G. A., & Zayats, A. V. (2012). Low-temperature plasmonics of metallic nanostructures. *Nano letters*, 12(3), 1561-1565.
- Cai, X., Zhang, P., Ma, L., Zhang, W., Ning, X., Zhao, L., & Zhuang, J. (2009). Tuning Optical Properties of Magic Number Cluster (SiO₂)₄₀H₄ by Substitutional Bonding with Gold Atoms. *The Journal of Physical Chemistry A*, 113(17), 4889-4894.
- Candido, L., Rabelo, J. T., Da Silva, J. L., & Hai, G.-Q. (2012). Quantum Monte Carlo study of small aluminum clusters Al_n (n= 2–13). *Physical Review B*, 85(24), 245404.
- Chen, J.-Q., Ping, J., & Wang, F. (1989). *Group representation theory for physicists* (Vol. 7): World Scientific.
- Chen, J., Wang, D., Xi, J., Au, L., Siekkinen, A., Warsen, A., . . . Li, X. (2007). Immuno Gold Nanocages with Tailored Optical Properties for Targeted Photothermal Destruction of Cancer Cells. *Nano Letters*, 7(5), 1318-1322.
- Chou, J., Hsing, C., Wei, C., Cheng, C., & Chang, C. (2013). Ab initio random structure search for 13-atom clusters of fcc elements. *Journal of Physics: Condensed Matter*, 25(12), 125305.
- Cramer, C. J. (2013). *Essentials of computational chemistry: theories and models*: John Wiley & Sons.

- De Heer, W. A. (1993). The physics of simple metal clusters: experimental aspects and simple models. *Reviews of Modern Physics*, 65(3), 611-676.
- Delley, B. (1990). An all-electron numerical method for solving the local density functional for polyatomic molecules. *The Journal of Chemical Physics*, 92(1), 508-517.
- Delley, B. (2000). From molecules to solids with the DMol3 approach. *The Journal of Chemical Physics*, 113(18), 7756-7764.
- Delley, B. (2002). Hardness conserving semilocal pseudopotentials. *Physical Review B*, 66(15), 155125.
- Derosa, P. A., Seminario, J. M., & Balbuena, P. B. (2001). Properties of Small Bimetallic Ni-Cu Clusters. *The Journal of Physical Chemistry A*, 105(33), 7917-7925.
- Dintinger, J., & Scharf, T. (2013). Plasmonic Nanoparticle-Based Metamaterials: From Electric to Magnetic Response *Amorphous Nanophotonics* (pp. 327-365): Springer.
- Drachev, V. P., Chettiar, U. K., Kildishev, A. V., Yuan, H.-K., Cai, W., & Shalaev, V. M. (2008). The Ag dielectric function in plasmonic metamaterials. *Optics express*, 16(2), 1186-1195.
- Draine, B. T., & Flatau, P. J. (1994). Discrete-Dipole Approximation For Scattering Calculations. *Journal of the Optical Society of America A*, 11(4), 1491-1499.
- Drude, P. (1900). Zur Elektronentheorie der Metalle. *Annalen der Physik*, 306(3), 566-613.
- Ebbesen, T. W., Lezec, H., Ghaemi, H., Thio, T., & Wolff, P. (1998). Extraordinary optical transmission through sub-wavelength hole arrays. *Nature*, 391(6668), 667-669.

- Elman, M., & Lebzelter, J. (2004). Light therapy in the treatment of acne vulgaris. *Dermatologic surgery*, 30(2), 139-146.
- Emsley, J. Oxford Chemistry Guides. *The Elements*, (ed. 2, Clarendon Press Oxford, 1991).
- Fahim, N., Ouyang, Z., Zhang, Y., Jia, B., Shi, Z., & Gu, M. (2012). Efficiency enhancement of screen-printed multicrystalline silicon solar cells by integrating gold nanoparticles via a dip coating process. *Optical Materials Express*, 2(2), 190-204.
- Fang, N., Lee, H., Sun, C., & Zhang, X. (2005). Sub-diffraction-limited optical imaging with a silver superlens. *Science*, 308(5721), 534-537.
- Ferrando, R., Jellinek, J., & Johnston, R. L. (2008). Nanoalloys: From Theory to Applications of Alloy Clusters and Nanoparticles. *Chemical Reviews*, 108(3), 845-910.
- Fournier, R., Zamiruddin, S., & Zhang, M. (2009). Competition between mixing and segregation in bimetallic Ag_nRb_n clusters (n= 2-10) 1, 2. *Canadian Journal of Chemistry*, 87(7), 1013-1021.
- Fuentealba, P., & Padilla-Campos, L. (2005). Electronic properties of small bimetallic LinCum (n, m ≤ 4) clusters. A comparison with Lin and Cun clusters. *International journal of quantum chemistry*, 102(5), 498-505.
- Fuller, C. C., Davis, J. A., & Waychunas, G. A. (1993). Surface chemistry of ferrihydrite: Part 2. Kinetics of arsenate adsorption and coprecipitation. *Geochimica et Cosmochimica Acta*, 57(10), 2271-2282.
- Garza, J., Nichols, J. A., & Dixon, D. A. (2000). The optimized effective potential and the self-interaction correction in density functional theory: Application to molecules. *The Journal of Chemical Physics*, 112(18), 7880-7890.
- Gross, E. K. U., & Kohn, W. (1990). Time-Dependent Density-Functional Theory. In L. Per-Olov (Ed.), *Advances in Quantum Chemistry* (Vol. Volume 21, pp. 255-291): Academic Press.

- Guvelioglu, G. H., Ma, P., He, X., Forrey, R. C., & Cheng, H. (2005). Evolution of small copper clusters and dissociative chemisorption of hydrogen. *Physical review letters*, *94*(2), 026103.
- Harb, M., Rabilloud, F., & Simon, D. (2010). Structural, electronic, magnetic and optical properties of icosahedral silver-nickel nanoclusters. *Physical Chemistry Chemical Physics*, *12*(16), 4246-4254. doi: 10.1039/B912971E
- Harb, M., Rabilloud, F., Simon, D., Rydlo, A., Lecoultre, S., Conus, F., . . . Félix, C. (2008). Optical absorption of small silver clusters: Ag_n (n=4–22). *The Journal of Chemical Physics*, *129*(19),
- Hearn, R. M. R., Kerr, A. C., Rahim, K., Ferguson, J., & Dawe, R. (2008). Incidence of skin cancers in 3867 patients treated with narrow-band ultraviolet B phototherapy. *British Journal of Dermatology*, *159*(4), 931-935.
- Janssens, E., Neukermans, S., Nguyen, H. M. T., Nguyen, M. T., & Lievens, P. (2005). Quenching of the Magnetic Moment of a Transition Metal Dopant in Silver Clusters. *Physical Review Letters*, *94*(11), 113401.
- Johnson, P. B., & Christy, R.-W. (1972). Optical constants of the noble metals. *Physical Review B*, *6*(12), 4370.
- Kaizuka, K., Miyamura, H., & Kobayashi, S. (2010). Remarkable Effect of Bimetallic Nanocluster Catalysts for Aerobic Oxidation of Alcohols: Combining Metals Changes the Activities and the Reaction Pathways to Aldehydes/Carboxylic Acids or Esters. *Journal of the American Chemical Society*, *132*(43), 15096-15098.
- Keast, V. J., Barnett, R. L., & Cortie, M. (2014). First principles calculations of the optical and plasmonic response of Au alloys and intermetallic compounds. *Journal of Physics: Condensed Matter*, *26*(30), 305501.
- Khanna, z. S., Rao, B., & Jena, P. (2002). Electronic signature of the magicity and ionic bonding in Al₁₃X (X= Li–K) clusters. *Physical Review B*, *65*(12), 125105.

- Kittel, C. (2005). *Introduction to Solid State Physics*.
- Koutchma, T., Forney, L. J., & Moraru, C. I. (2009). *Ultraviolet light in food technology: principles and applications*: CRC Press.
- Kroner, M., Govorov, A., Remi, S., Biedermann, B., Seidl, S., Badolato, A., . . . Gerardot, B. (2008). The nonlinear Fano effect. *Nature*, *451*(7176), 311-314.
- Kumar, V. (1998). Structure and electronic properties of Al₁₄ and Al₁₃ Na clusters. *Physical Review B*, *57*(15), 8827.
- Kunz, K. S., & Luebbers, R. J. (1993). *The finite difference time domain method for electromagnetics*: CRC press.
- Lee, Y. J., Lee, Y., Oh, D., Chen, T., Ceder, G., & Belcher, A. M. (2010). Biologically activated noble metal alloys at the nanoscale: for lithium ion battery anodes. *Nano Letters*, *10*(7), 2433-2440.
- Lezec, H. J., Dionne, J. A., & Atwater, H. A. (2007). Negative refraction at visible frequencies. *Science*, *316*(5823), 430-432.
- Li, C.-G., Zhou, X.-W., Tang, Y.-N., Chen, W.-G., Pan, L.-J., & Kuang, X.-Y. (2015). Structures, stabilities and electronic properties of Cu_nNa (n= 1–8) clusters. *Computational and Theoretical Chemistry*, *1055*, 51-60.
- Lin, Y.-C., Sundholm, D., Juselius, J., Cui, L.-F., Li, X., Zhai, H.-J., & Wang, L.-S. (2006). Experimental and computational studies of alkali-metal coinage-metal clusters. *The Journal of Physical Chemistry A*, *110*(12), 4244-4250.
- Liu, Z., Lee, H., Xiong, Y., Sun, C., & Zhang, X. (2007). Far-field optical hyperlens magnifying sub-diffraction-limited objects. *Science*, *315*(5819), 1686-1686.
- Ma, W., & Chen, F. (2012). Optical and electronic properties of Cu doped Ag clusters. *Journal of Alloys and Compounds*, *541*(0), 79-83.

- Ma, W., & Chen, F. (2013). Electronic, magnetic and optical properties of Cu, Ag, Au-doped Si clusters. *Journal of molecular modeling*, 19(10), 4555-4560.
- Manolopoulos, D. E., May, J. C., & Down, S. E. (1991). Theoretical studies of the fullerenes: C₃₄ to C₇₀. *Chemical physics letters*, 181(2), 105-111.
- Marques, M. A., Maitra, N. T., Nogueira, F. M., Gross, E. K., & Rubio, A. (2012). *Fundamentals of time-dependent density functional theory* (Vol. 837): Springer.
- Marton, J., & Jordan, B. (1977). Optical properties of aggregated metal systems: interband transitions. *Physical Review B*, 15(4), 1719.
- Mertens, H., Koenderink, A., & Polman, A. (2007). Plasmon-enhanced luminescence near noble-metal nanospheres: Comparison of exact theory and an improved Gersten and Nitzan model. *Physical Review B*, 76(11), 115123.
- Michaelian, K., Rendón, N., & Garzón, I. L. (1999). Structure and energetics of Ni, Ag, and Au nanoclusters. *Physical Review B*, 60(3), 2000-2010.
- Mie, G. (1908). Contribution to the optical properties of turbid media, in particular of colloidal suspensions of metals. *Ann. Phys.(Leipzig)*, 25, 377-452.
- Molina, L. M., & Hammer, B. (2005). The activity of the tetrahedral Au₂₀ cluster: charging and impurity effects. *Journal of Catalysis*, 233(2), 399-404.
- Naik, G., Kim, J., Kinsey, N., & Boltasseva, A. (2014). Chapter 6 - Alternative Plasmonic Materials. In N. V. Richardson & H. Stephen (Eds.), *Handbook of Surface Science* (Vol. Volume 4, pp. 189-221): North-Holland.
- Naik, G. V., Shalaev, V. M., & Boltasseva, A. (2013). Alternative plasmonic materials: beyond gold and silver. *Advanced Materials*, 25(24), 3264-3294.

- Neogrady, P., Kello, V., Urban, M., & Sadlej, A. J. (1998). Ionization potentials and electron affinities of Cu, Ag, and Au: Electron correlation and relativistic effects. *International journal of quantum chemistry*(63), 557-565.
- Oates, T., & Mucklich, A. (2005). Evolution of plasmon resonances during plasma deposition of silver nanoparticles. *Nanotechnology*, 16(11), 2606.
- Ouyang, Y., Wang, P., Xiang, P., Chen, H., & Du, Y. (2012). Density-functional theory study of Al_n and Al_n-1 Mg (n= 2–17) clusters. *Computational and Theoretical Chemistry*, 984, 68-75.
- Perdew, J. P., Burke, K., & Ernzerhof, M. (1996). Generalized Gradient Approximation Made Simple. *Physical Review Letters*, 77(18), 3865-3868.
- Pereiro, M., & Baldomir, D. (2007). Structure of small silver clusters and static response to an external electric field. *Physical Review A*, 75(3), 033202.
- Persson, B. (1991). Surface resistivity and vibrational damping in adsorbed layers. *Physical Review B*, 44(7), 3277.
- Photiphitak, C., Rakkwamsuk, P., Muthitamongkol, P., Sae-Kung, C., & Thanachayanont, C. (2011). Effect of silver nanoparticle size on efficiency enhancement of dye-sensitized solar cells. *International Journal of Photoenergy*, 2011.
- Pietrobon, B., & Kitaev, V. (2008). Photochemical synthesis of monodisperse size-controlled silver decahedral nanoparticles and their remarkable optical properties. *Chemistry of Materials*, 20(16), 5186-5190.
- Pilgrim, J. S., & Duncan, M. A. (1995). Photoionization spectroscopy of AgLi. *Chemical Physics Letters*, 232(4), 335-340.
- Pillai, S., Catchpole, K. R., Trupke, T., & Green, M. A. (2007). Surface plasmon enhanced silicon solar cells. *Journal of Applied Physics*, 101(9), 093105.

- Prasad, N. E., Gokhale, A., & Wanhill, R. (2013). *Aluminum-Lithium Alloys: Processing, Properties, and Applications*: Butterworth-Heinemann.
- Rao, B. K., & Jena, P. (1999). Evolution of the electronic structure and properties of neutral and charged aluminum clusters: A comprehensive analysis. *The Journal of Chemical Physics*, *111*(5), 1890-1904.
- Rao, Y., Lei, Y., Cui, X., Liu, Z., & Chen, F. (2013). Optical and magnetic properties of Cu-doped 13-atom Ag nanoclusters. *Journal of Alloys and Compounds*, *565*(0), 50-55.
- Rashid, M. H., & Mandal, T. K. (2007). Synthesis and catalytic application of nanostructured silver dendrites. *The Journal of Physical Chemistry C*, *111*(45), 16750-16760.
- Rodriguez, J. A., & Goodman, D. W. (1992). The Nature of the Metal-Metal Bond in Bimetallic Surfaces. *Science*, *257*(5072), 897-903.
- Schwartzberg, A. M., & Zhang, J. Z. (2008). Novel Optical Properties and Emerging Applications of Metal Nanostructures†. *The Journal of Physical Chemistry C*, *112*(28), 10323-10337.
- Shalaev, V. M., Cai, W., Chettiar, U. K., Yuan, H.-K., Sarychev, A. K., Drachev, V. P., & Kildishev, A. V. (2005). Negative index of refraction in optical metamaterials. *Optics letters*, *30*(24), 3356-3358.
- Singh, D., Rathod, V., Ninganagouda, S., Hiremath, J., Singh, A. K., & Mathew, J. (2014). Optimization and Characterization of Silver Nanoparticle by Endophytic Fungi *Penicillium* sp. Isolated from *Curcuma longa* (Turmeric) and Application Studies against MDR *E. coli* and *S. aureus*. *Bioinorganic chemistry and applications*, 2014.
- Smith, D. D., Yoon, Y., Boyd, R. W., Campbell, J. K., Baker, L. A., Crooks, R. M., & George, M. (1999). z-scan measurement of the nonlinear absorption of a thin gold film. *Journal of Applied Physics*, *86*(11), 6200-6205.

- Stangassinger, A., Knight, A. M., & Duncan, M. A. (1997). Photoionization spectroscopy of NaAg. *Chemical Physics Letters*, 266(1–2), 189-194.
- Thayer, J. S. (2010). Relativistic effects and the chemistry of the heavier main group elements *Relativistic Methods for Chemists* (pp. 63-97): Springer.
- Tobiška, P., Hugon, O., Trouillet, A., & Gagnaire, H. (2001). An integrated optic hydrogen sensor based on SPR on palladium. *Sensors and Actuators B: Chemical*, 74(1), 168-172.
- Tozer, D. J. (2003). Relationship between long-range charge-transfer excitation energy error and integer discontinuity in Kohn–Sham theory. *The Journal of Chemical Physics*, 119(24), 12697-12699.
- Tozer, D. J., & De Proft, F. (2005). Computation of the hardness and the problem of negative electron affinities in density functional theory. *The Journal of Physical Chemistry A*, 109(39), 8923-8929.
- Trivedi, N., & Ashcroft, N. (1988). Quantum size effects in transport properties of metallic films. *Physical Review B*, 38(17), 12298.
- Weaver, J., & Frederikse, H. (2001). Optical properties of selected elements. *CRC Handbook of Chemistry and Physics*, CRC Press, Boca Raton, 12-133.
- Wei, H., & Eilers, H. (2009). From silver nanoparticles to thin films: Evolution of microstructure and electrical conduction on glass substrates. *Journal of Physics and Chemistry of Solids*, 70(2), 459-465.
- Weissker, H.-C., & Mottet, C. (2011). Optical properties of pure and core-shell noble-metal nanoclusters from TDDFT: The influence of the atomic structure. *Physical Review B*, 84(16), 165443.
- West, P. R., Ishii, S., Naik, G. V., Emani, N. K., Shalaev, V. M., & Boltasseva, A. (2010). Searching for better plasmonic materials. *Laser & Photonics Reviews*, 4(6), 795-808. doi: 10.1002/lpor.200900055

- Wilson, E. B., Decius, J., & Cross, P. C. (1955). The theory of infrared and Raman vibrational spectra *Molecular Vibrations*: McGraw-Hill New York.
- Yagil, Y., Gadenne, P., Julien, C., & Deutscher, G. (1992). Optical properties of thin semicontinuous gold films over a wavelength range of 2.5 to 500 *Physical Review B*, 46(4), 2503-2511.
- Yang, M., Jackson, K. A., & Jellinek, J. (2006). First-principles study of intermediate size silver clusters: Shape evolution and its impact on cluster properties. *The Journal of Chemical Physics*, 125(14).
- Yang, Z.-J., Zhang, Z.-S., Zhang, L.-H., Li, Q.-Q., Hao, Z.-H., & Wang, Q.-Q. (2011). Fano resonances in dipole-quadrupole plasmon coupling nanorod dimers. *Optics letters*, 36(9), 1542-1544.
- Yeh, C. S., Robbins, D. L., Pilgrim, J. S., & Duncan, M. A. (1993). Photoionization electronic spectroscopy of AgK. *Chemical Physics Letters*, 206(5-6), 509-514.
- Yildirim, H., Kara, A., & Rahman, T. S. (2011). Tailoring Electronic Structure Through Alloying: The Ag_nCu_{34-n} (n = 0-34) Nanoparticle Family. *The Journal of Physical Chemistry C*, 116(1), 281-291.
- Yu, A. K., Kudrinskiy, A. A., Olenin, A. Y., & Lisichkin, G. V. (2008). Synthesis and properties of silver nanoparticles: advances and prospects. *Russian Chemical Reviews*, 77(3), 233.
- Yuan, D., Gong, X., & Wu, R. (2008). Peculiar distribution of Pd on Au nanoclusters: First-principles studies. *Physical Review B*, 78(3), 035441.
- Yuan, D. W., Wang, Y., & Zeng, Z. (2005). Geometric, electronic, and bonding properties of Au_NM (N=1-7, M=Ni, Pd, Pt) clusters. *The Journal of Chemical Physics*, 122(11).

- Zeng, S., Yong, K.-T., Roy, I., Dinh, X.-Q., Yu, X., & Luan, F. (2011). A Review on Functionalized Gold Nanoparticles for Biosensing Applications. *Plasmonics*, 6(3), 491-506.
- Zhan, C.-G., Nichols, J. A., & Dixon, D. A. (2003). Ionization potential, electron affinity, electronegativity, hardness, and electron excitation energy: molecular properties from density functional theory orbital energies. *The Journal of Physical Chemistry A*, 107(20), 4184-4195.
- Zhang, G., & Musgrave, C. B. (2007). Comparison of DFT Methods for Molecular Orbital Eigenvalue Calculations. *The Journal of Physical Chemistry A*, 111(8), 1554-1561.
- Zhang, Y., Ouyang, Z., Stokes, N., Jia, B., Shi, Z., & Gu, M. (2012). Low cost and high performance Al nanoparticles for broadband light trapping in Si wafer solar cells. *Applied Physics Letters*, 100(15), 151101.
- Zhurkin, E. E., Van Hoof, T., & Hou, M. (2007). Nanoscale alloys and core-shell materials: Model predictions of the nanostructure and mechanical properties. *Physical Review B*, 75(22), 224102.